Clustering: a rational design principle for potentiated antibody therapeutics

Oostindie, S.C.

5

THERAPEUTIC IGG ANTIBODY COMBINATIONS ACTING AS BIO-LOGIC AND GATES

Simone C. Oostindie[1,2], Frank J. Beurskens[1], Gijs G. Zom[1], Desiree Paulet[1], Kusai Al-Tamimi[1], Els van der Meijden[1], Jennifer Scheick[1], Janita J. Oosterhoff[1], Julie Vignau[1], Sandra Verploegen[1], Janine Schuurman[1], Rob N. de Jong[1*]

Submitted for publication.

1 Genmab, Uppsalalaan 15, 3584 CT Utrecht, The Netherlands
2 Department of Immunology, Leiden University Medical Center, Leiden, The Netherlands
* Corresponding author

Correspondence
Rob N. de Jong (rjo@genmab.com)

Acknowledgements
We thank Klara Beslmüller and Tessa Wilpshaar for experimental support.

ABSTRACT

The target space for therapeutic monoclonal antibodies is limited by expression in healthy tissues. We present a general approach to enhance functional selectivity by decoupling activity from individual antibody binding events. Immunoglobulin G (IgG)-mediated clustering of membrane receptors naturally occurs on cell surfaces to trigger complement- or cell-mediated effector functions, but can also be leveraged to initiate outside-in signaling. Here, we describe Fc-domain engineered IgG antibody pairs that act as Bio-Logic AND gates selectively activated after hetero-oligomerization. Pairwise IgG hetero-oligomerization and membrane receptor activation were stringently dependent on the presence of two targets co-expressed at the same cell surface. C1q recruitment integrated the binding signals encoded by two antibody components, translating into clustering-dependent activation of effector functions such as complement activity or target signaling. This 'HexElect®' technology may enable access to an untapped, combinatorial target space for the generation of antibody therapeutics that exhibit both selectivity and potency.

Monoclonal antibodies (mAbs) have reshaped drug development due to their highly targeted nature and their ability to activate specific immune effector molecules and cells. Superior effector functions have been engineered into mAbs to enhance therapeutic efficacy[1]. Complement- or cell-mediated effector functions can be triggered by antigen-dependent Immunoglobulin G (IgG) oligomerization into ordered hexameric complexes on the cell surface through non-covalent Fc-Fc interactions between neighboring antibodies[2]. These ordered hexamers provide natural high-avidity binding sites for complement complex C1, leading to activation of the classical complement pathway, or to receptor clustering and outside-in signaling[3-6]. IgG hexamerization and effector function activation can be enhanced by single amino acid point mutations in the Fc-domain, such as E430G, that promote interactions between Fc domains of cell-bound IgG[2,7]. Hexamerization-enhanced mutant antibody variants increased complement-dependent cytotoxicity (CDC) of B cells from patients with chronic lymphocytic leukemia (CLL) and were able to facilitate enhanced clustering and activation of members of the tumor necrosis factor receptor (TNFR) superfamily[3,6,8].

The cell surface target space for therapeutic mAbs based on natural IgG backbones is largely limited to those targets that are highly selectively expressed on diseased cells. Hence, there may be advantages to therapeutic antibody technologies that enable the safe and effective targeting of antigens that currently cause undesirable toxicity on healthy cells, or insufficient potency on

diseased cells. We recently reported that mAbs targeting different membrane receptors can hetero-oligomerize into mixed hexameric complexes upon antigen binding, resulting in synergistic CDC of tumor B cells from various B-cell malignancies[8]. Here, we describe a general approach to create IgG antibody pairs that only induce pairwise activation of enhanced, hexamerization-dependent functions, if both antibodies have bound the same target cell. Decoupling functional activation from individual target binding enables these IgG antibody pairs to act as Boolean logic AND gates that integrate two antibody binding signals into a functional outcome only on cells or surfaces co-expressing both antibody targets.

METHODS

Antibodies

Rituximab (MabThera®) and obinutuzumab (Gazyvaro®) were obtained from the pharmacy (UMC Utrecht). All other antibodies were recombinantly produced at Genmab as described.[3] Mutations to enhance or inhibit Fc-Fc interactions and/or Fc-C1q binding interactions were introduced in expression vectors encoding the antibody heavy chain either using Quikchange technology (Agilent Technologies, Santa Clara, CA, USA) or via gene synthesis (Thermofisher Scientific, Regensburg, Germany). Quality control of recombinantly produced antibodies was performed by different methods as described previously[7]: capillary electrophoresis sodium dodecyl sulfate (CE-SDS) on the Labchip GXII (Caliper Life Sciences/PerkinElmer Hopkinton) under reducing and non-reducing conditions (>90% intact IgG, >95% HC þ LC under reducing conditions), Electrospray Ionization Time-of-Flight Mass Spectrometry (ESI-TOF MS) (Waters) or Orbitrap (Thermo Fisher Scientific), and High performance size-exclusion chromatography (HP-SEC) (aggregate level < 5%; Waters Alliance 2975 separation unit, Waters). The following IgG1 antibodies targeting human antigens were used: CD52 (P31358) mAb Campath[37], CD20 (P11836) mAbs 11B8 and 7D8[38-40], CD3 (P07766) mAb huCLB3/4[41], CD37 (P11049) mAb IgG1-37.3[42], DR5 (O14763) mAbs DR5-01 and DR5-05[3]. mAb IgG1-b12 targeting HIV-1 antigen gp120 (Q9IZE4) was used as a non-binding isotype control.[43]

Cells and reagents

Daudi (human B-cell lymphoma), Raji (human B-cell lymphoma), Ramos (human B-cell lymphoma), COLO-205 (colorectal cancer) and BxPC-3 (pancreatic cancer) cell lines were obtained from the American Type Culture Collection (ATCC no. CCL-23, CCL-86, CRL-1596, CCL-222 and CRL-1687 respectively). The human B-lymphoma cell line U-698-M and the human B-precursor leukemia cell line REH were obtained from the Deutsche Sammlung von Mikroorganismen und Zellkulturen (cell line numbers ACC 22 and ACC 4 respectively; Braunschweig, Germany). Wien-133 cells (human Burkitt's lymphoma) were kindly provided by Dr. Geoff Hale (BioAnaLab Limited, Oxford, UK).

PBMCs derived from CLL patients were commercially obtained from Discovery Life Sciences (Huntsville, AL, USA). Buffy coats from healthy human donors and complement-competent, pooled normal human serum (NHS; AB positive) were obtained from Sanquin (Amsterdam, The Netherlands). Whole blood samples from healthy human volunteers were freshly obtained from the University Medical Center Utrecht (Netherlands). Purified C1q protein and C1

complex were obtained from Quidel (San Diego, CA, USA) and Complement Technology (Tyler, TX, USA) respectively.

Whole blood cytotoxicity

Cytotoxicity assays were performed with healthy human donor blood samples that were hirudin anticoagulated or EDTA anticoagulated and recalcified using 5 mM $CaCl_2$ (Sigma Aldrich) for 30 minutes in the presence of 10 µg/mL hirudin (Genscript) to preserve complement activity. Briefly, whole blood was incubated with antibodies for 45 minutes or 18 hours at 37 °C 5% CO_2. After 45 minutes incubation, samples were stained for 30 minutes at 4 °C with fluorochrome-labeled lineage-specific antibodies and fixable viability stain (FVS-BV510; BD) to characterize cell subsets and dead or dying cells, respectively. Next, red blood cells were lysed (lysis buffer: 10 mM KHCO3, 0.01 mM EDTA and 155 mM NH4Cl) and cells were fixed in 2% paraformaldehyde before measuring on a flow cytometer. After 18 hours incubation, red blood cells were lysed first and next samples were stained as described above, before measuring on an LSRFortessa (BD Biosciences, Franklin Lakes, NJ, USA) flow cytometer. Cell markers used to define cell populations were: CD45-PerCP (Biolegend, San Diego, CA, USA), CD66b-PE-Cy7 (Biolegend), CD3-eFluor450 (Waltham, MA, USA), CD4-APC-eFluor780 (eBioscience, San Diego, CA, USA) and CD19-BV711 (Biolegend). The gating strategy used to define cell populations is described in Supplementary Figure 7A. Cytotoxicity was calculated as the fraction (%) of cells remaining after treatment relative to a non-treated control sample (100%).

C1q binding

Wien-133 cells were opsonized with antibody serial dilutions for 15 min at 37 °C. Subsequently, cells and antibodies were put on ice, purified human complement component C1q (2.5 µg/mL) was added and incubated for 45 min. After washing, C1q binding was detected using a Fluorescein isothiocyanate (FITC) conjugated rabbit anti-human C1q antibody (Dako, Glostrup, Denmark) and quantified as the FITC geometric mean fluorescent intensity (gMFI) determined an iQue Screener flow cytometer (Sartorius, Göttingen, Germany).

CDC

CDC assays were performed using tumor cells incubated with antibody concentration series or a fixed antibody concentration as indicated, for 45 minutes at 37 °C in the presence of normal human serum (NHS; 20% final concentration) as source of complement. Killing was calculated as the fraction of propidium iodide (PI)-positive cells (%) determined by an iQue Screener flow cytometer for B-tumor cell lines and as the fraction of TO-PRO-3-positive cells (%) determined by an LSRFortessa flow cytometer for $CD19^+$ CLL B cells.

FcγR binding

Binding of antibody variants to the monomeric extracellular domain (ECD) of FcγRIA (FCGR1AECDHis) and to dimeric ECDs of FcγRIIA allotype 131H (diFCGR2AH-HisBAP), FcγRIIA allotype 131R (diFCGR2AR-HisBAP), FcγRIIIA allotype 158F (diFCGR3AF-HisBAP), and FcγRIIIA allotype 158V (diFCGR3AV-HisBAP) was tested in ELISA assays.[44] For binding to dimeric FcγR variants, 100 µL goat anti-human F(ab›)2 (1 µg/mL) was added per well for coating overnight at 4 °C. After washing the plates, non-specific binding was blocked for 1 hour at room temperature (RT) by adding 200 µL/well PBS/0.2% BSA. With washings in between incubations, plates were sequentially incubated with 100 µL of 20 µg/mL antibody variants in PBST with 0.2% BSA buffer for 1 hour at RT, 100 µL of the recombinant dimeric FcγR constructs (1 µg/mL) for 1 hour at RT, and 100 µL streptavidin-labelled Poly-HRP (1:10.000) for 30 minutes at RT. Development was performed for 10-30 minutes with 1 mg/mL ABTS (Roche, Mannheim, Germany). To stop the reactions, 100 µL/well of 2% oxalic acid was added. Absorbance was measured at 405 nm in a microplate reader (BioTek, Winooski, VT, USA). To detect binding to monomeric FcγRIa, plates were coated with monomeric his-tagged FCGR1A ECD and after antibody incubation, goat anti-human-kappaLC-HRP (1:5000) was used as detection antibody.

FcγR activation

Activation of FcγRIIa- (allotype H-131) and FcγRIIIa-mediated (allotype V-158) intracellular signaling was quantified using Luminescent Reporter Bioassays (Promega, Madison, WI, USA), according to the manufacturer's recommendations.

ADCC

ADCC was assessed using a DELFIA® EuTDA Cytotoxicity assay (PerkinElmer, Norwalk, CT, USA) according to the manufacturer's recommendations. Briefly, Wien-133 target cells were loaded with BATDA reagent, and 1E+04 cells were incubated with antibody serial dilutions and human healthy donor PBMCs (isolated from buffy coats through centrifugation using Leucosep™ tubes according to the manufacturer's instructions; Greiner Bio-one) as effector cells, at a 100:1 effector to target ratio, for 2 hours at 37 °C in a total volume of 160 µL. After incubation and centrifugation, 20 µL of supernatant was transferred to a 96 well plate, 200 µL Europium Solution was added, and the mixture was incubated for 15 min at RT while shaking. EuTDA release and time-resolved fluorescence was measured on an EnVision Multilabel Reader (PerkinElmer). Maximal and spontaneous release were determined using target cells incubated with 0.1% Triton X-100 or target cells in medium without effector cells, respectively. Specific release was calculated as:

$$\% \text{ specific release} = 100 * \frac{(\text{counts release sample-counts spontaneous release})}{(\text{counts maximal release-counts spontaneous release})}$$

ADCP

ADCP assays were performed as described[45]. In short, human $CD14^+$ monocytes were obtained from healthy donor PBMCs (isolated from buffy coats through centrifugation using Leucosep™ tubes according to the manufacturer's instructions) through positive isolation using CD14 MicroBeads (Miltenyi Biotec, Leiden, Netherlands) according to the manufacturer's instructions. Monocytes were cultured in culture medium (CellGenix® GMP DC serum-free medium with 50 ng/ml M-CSF) in Nunc™ dishes with UpCell™ surface (Thermo Fisher Scientific) at 37 ˚C/5% CO_2 for 7-8 days to obtain human monocyte-derived macrophages (h-MDM). h-MDMs were characterized by flow cytometry for expression of myeloid- and macrophage-specific maturation markers (Supplementary Table 1). ADCP was determined using Raji cells labeled with calcein AM (Life Technologies, Carlsbad, CA, USA) according to the manufacturer's instructions and opsonized with antibodies for 15 minutes at 37°C. h-MDM were added at an effector to target (E:T) ratios of 2:1 and incubated for 4 hours at 37 °C/5% CO_2. After incubation, tumor cells and h-MDM were stained for surface markers using fluorochrome-conjugated antibodies (Supplementary Table 2) for 30 minutes at 4 °C and analyzed on an LSR-Fortessa flow cytometer. The gating strategy used to define cell populations is described in Supplementary Figure 7B. ADCP was calculated as the fraction of $CD11b^+$/calcein AM^+/$CD19^-$ cells within the total hMDM ($CD11b^+$) cell population.

Target expression

Expression levels of cellular markers were determined using an indirect immunofluorescence assay (QIFIKIT®, Agilent Technologies, Santa Clara, CA, USA and Human IgG Calibrator kit, BioCytex, Marseille, France) according to the manufacturer's instructions.

FRET

Proximity-induced FRET was determined by measuring energy transfer between cells incubated with A555-conjugated donor and A647-conjugated acceptor mAbs using flow cytometry as described.[8,21] Briefly, purified B cells (isolated from buffy coats using Dynal Dynabeads Untouched Human B cell isolation kit (Life Technologies) according to manufacturer instructions) were incubated with A555-conjugated donor mAbs and/or A647-conjugated acceptor mAbs in the presence or absence of purified human C1q (Quidel; 2.5 µg/

mL) or C1 (Complement Technology; 2.42 µg/mL). gMFI values were measured using an LSRFortessa flow cytometer by recording events at 585/42 nm (FL2, donor A488) and ≥670 nm (FL3), both excited at 488 nm, and at 660/20 nm (FL4, acceptor A647), excited at 635 nm. Unquenched donor fluorescence intensity was determined with cells incubated with A555-conjugated donor mAbs, and non-enhanced acceptor intensity was determined with cells incubated with A647-conjugated acceptor mAbs. Proximity-induced FRET was determined by measuring energy transfer between cells incubated with A555-conjugated donor and A647-conjugated acceptor mAbs. gMFI values allowed calculation of FRET according to the following equation:

$$\text{Energy transfer (ET)} = \text{FL3(D, A)} - \frac{\text{FL2(D, A)}}{\text{(a)}} - \frac{\text{FL4(D, A)}}{\text{(b)}}$$

Wherein a = FL2(D)/FL3(D), b = FL4(A)/FL3(A), D is donor, A is acceptor and FLn (D, A) = donor + acceptor.

ET values obtained were normalized:

$$\text{Normalized ET (\%)} = 100 * \frac{\text{ET}}{\text{FL3(D,A)}}$$

Viability assay

Cell viability was determined using a CellTiter-Glo® luminescent cell viability assay, according to the supplier's protocol (Promega, Madison, WI, USA). Cells were seeded in white OptiPlates (PerkinElmer) and allowed to adhere overnight at 37 °C. The following day, antibody serial dilutions and purified human C1q (Complement Technology; 2.5 µg/mL) were added and incubated for 3 days at 37°C. 5 µM staurosporine treated cells and untreated cells were included as positive and negative controls of cell death induction, respectively. After incubation, Luciferin Solution Reagent was added and plates were incubated for 1.5 hours at 37°C. Luminescence was measured on an EnVision Multilabel Reader. The percentage of viable cells was calculated using the following formula:

$$\text{\% viable cells} = 100 * \frac{\text{T-P}}{\text{V-P}}$$

Wherein T = luminescence of the test sample, P = luminescence of staurosporine control sample and V = luminescence of the medium control sample.

Animals

Animal experiments were performed in compliance with the Dutch animal protection law (WoD) translated from the directives (2010/63/EU) and if applicable, the Code of Practice "animal experiments for cancer research" (Inspection V&W, Zutphen, The Netherlands, 1999) and were approved by the Dutch Central Committee for animal experiments and by the local Ethical committee. Animals were housed and handled in accordance with good animal practice as defined by the Federation of European Laboratory Animal Science Associations (FELASA), in an association for assessment and accreditation of laboratory animal care (AAALAC) and ISO 9001:2000 accredited animal facility (GDL, Utrecht, Netherlands).

Pharmacokinetic analysis

Pharmacokinetic studies were performed using 11-12 weeks old female tumor-free C.B-17/IcrHan®Hsd-Prkdcscid mice (SCID, Envigo). Mice were injected intravenously (IV) with a single dose of 500 µg of each test reagent per mouse (n=3). Blood samples were drawn from the saphenous vein at 10 min, 4 h and 1, 2, 7, 14 and 21 days after antibody administration and collected into heparin-containing vials. Vials were centrifuged (10 min at 14.000 x g) to separate plasma from cells and plasma was stored at -20°C until further use. Total human IgG concentration in plasma samples was analyzed by ELISA. Plates were coated overnight at 4°C with 2 µg/mL of an in-house generated mouse-anti-human IgG2 recombinant Fab fragment in PBS and plasma human IgG was detected by a peroxidase-conjugated AffiniPure goat anti-human IgG Fcγ-specific antibody (Jackson, West Grace, PA, USA). Area under the curve (AUC) up to day 21 was determined using Graphpad Prism and clearance was calculated as (Dose (mg.kg−1) * 1,000 / AUC).

Data processing

Flow cytometry data were analyzed using FlowJo V10 software. Graphs were plotted and analyzed using GraphPad Prism 8.0. Dose-response curves were generated using best-fit values of non-linear dose-response fits using log-transformed concentrations. All data shown are representative of at least three independent replicate experiments or three individual human donors tested. The mean area under the curve (AUC) ± standard deviation (SD) was determined for all available dose-response analyses and is summarized in Supplementary Table 3. Dose-response data from multiple experimental repeats were pooled, concentrations were log-transformed and the resulting AUC values were normalized relative to the positive control indicated (100%) and negative control non-binding antibody IgG1-b12 (0%). The datasets generated during and/or analyzed during the current study are available from the corresponding author on reasonable request.

RESULTS

Combinations of CD52 and CD20 antibodies induce broad depletion of multiple hematological cell subsets

Previously, we showed that mutating amino acid positions Lys^{439} and Ser^{440} at the Fc-Fc interface into glutamate (K439E) and lysine (S440K), respectively, creates a pair of antibody mutants that show reduced self-oligomerization into homo-hexamers, but efficiently form hetero-hexamers in mixtures containing both mutants (Supplementary Figure 1)[2,8]. Here, we investigated if these mutations can be used to create antibody pairs targeting two different antigens that form hetero-hexameric complexes only when bound to the same target cell, enabling them to act as biologic equivalents of logic AND gates. These mutually dependent antibody pairs aim to activate effector functions only on cells expressing a combination of two targets A AND B, while preventing activation on cells expressing only target A or target B (Figure 1A-B).

To engineer antibody pairs that enable strictly mutually dependent activation, we chose a model system composed of antibodies targeting the abundantly expressed and well-characterized surface antigens CD52 and CD20. We generated hexamerization-enhanced (E430G) IgG1 antibodies that target CD52 (IgG1-Campath-E430G), expressed on various hematological cell subsets including T cells and B cells[9], and CD20 (IgG1-11B8-E430G), primarily expressed on B cells[10]. A mixture of IgG1-Campath-E430G and IgG1-11B8-E430G efficiently killed Wien-133 lymphoma B cells and depleted both B cells and T cells in human whole blood (Figure 2A, Supplementary Figure 2A). We tested if introducing mutations K439E and S440K (IgG1-Campath-E430G-K439E and IgG1-11B8-E430G-S440K) could induce selective kill of B cells expressing both CD52 and CD20, while sparing T cells expressing only CD52. However, antibody combination IgG1-Campath-E430G-K439E and IgG1-11B8-E430G-S440K (Figure 2A) killed both B cells and T cells in human whole blood at antigen saturation, indicating residual effector function activation and non-selective cell depletion. When tested individually, in the presence of a non-binding control antibody (IgG1-b12) to keep IgG concentrations directly comparable, both single agents (Figure 2A) displayed substantial residual activity in whole blood. Analysis of individual antibody effector functions in B-lymphoma cell lines demonstrated that IgG1-Campath-E430G-K439E still induced residual complement activation (Figure 2B), while IgG1-Campath-K439E without the E430G mutation did not, indicating that selectivity was lost when Fc-Fc interactions were promoted (Supplementary Figure 2B). Furthermore, both single components IgG1-Campath-E430G-K439E and IgG1-11B8-E430G-S440K still activated FcγRIIa- and FcγRIIIa-dependent signaling in

A

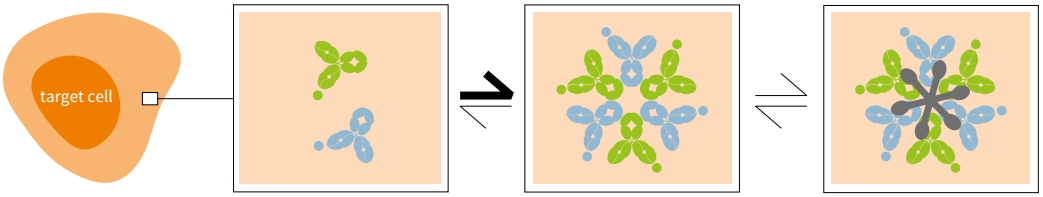

B

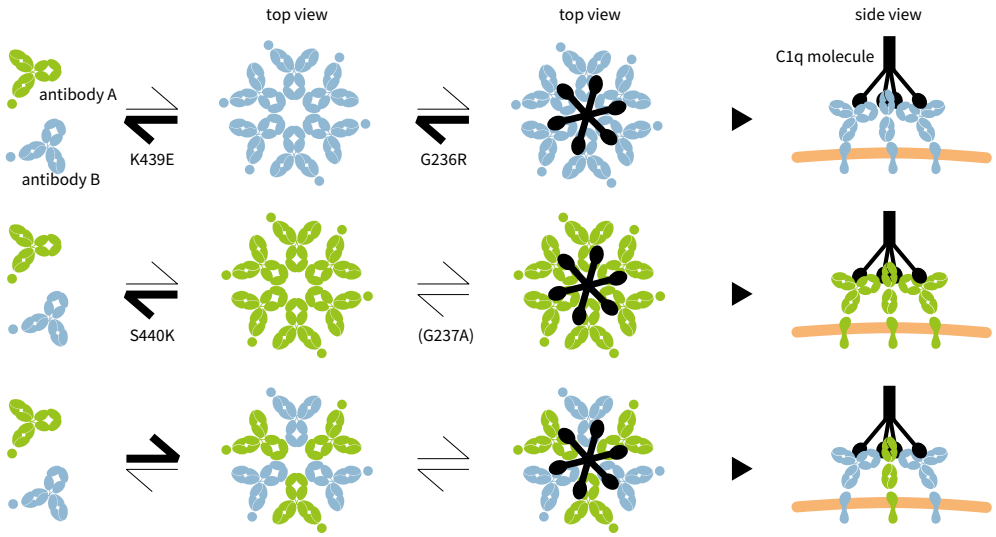

C

target A	target B	activity	
0	0	0	
1	0	0	
0	1	0	
1	1	1	

D

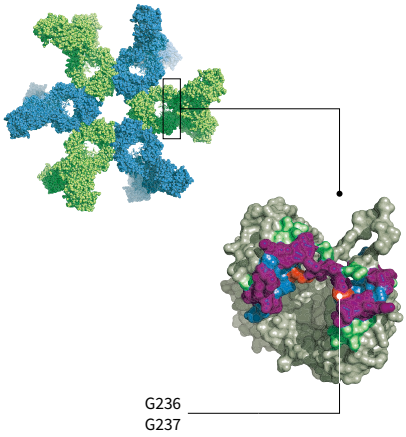

◀ **Figure 1**

Design of Fc-domain engineered IgG antibody pairs acting as Boolean logic AND gates.
(**A**) Schematic of antibody combinations that contain Fc domain modifications designed to induce hetero-hexamer formation only after cell surface target binding, aiming to recruit complement component C1q and induce effector function activation. (**B**) Mutually dependent antibody pairs may act as Bio-Logic AND gates by integrating two antibody-binding input signals into a functional output exclusively on cells or surfaces that co-express both antibody targets. (**C**) Summary of coupled biochemical equilibria illustrating how IgG1-hexamer-C1q avidity can be tuned using K439E/S440K and G236R/G237A mutations to favor hetero-hexamerization over homo-hexamerization. (**D**) Top left: overview of an IgG1 antibody hetero-hexamer based on the IgG1-b12 crystal structure (1HZH).[46] Bottom right: detailed view of an Fc hinge domain indicating amino acid positions involved in C1q- (green) and FcγR binding (blue). The largely shared C1q- and FcγR binding interface (purple) highlights preferred amino acid positions that differentially modulate C1q and FcγR binding (orange).

cell-based reporter assays (Figure 2C-D), suggesting that their activation was not strictly dependent on antibody hexamerization. Thus, this pair of antibody variants did not act in a strictly mutually dependent fashion, since the selective activation of effector functions by K439E and S440K mutant antibody pairs was compromised both by residual antibody clustering on single target cells, and by FcγR activity that was independent of antibody hexamerization.

G236/G237 mutations can differentially modulate multiple IgG1 effector functions

To increase the selectivity of effector function activation by K439E and S440K mutant antibody pairs, we differentially modulated the binding to FcγR and C1q effector molecules (Figure 1C). IgG (hetero-) hexamer abundance and stability are the product of both Fc-Fc and Fc-C1q interactions[2,5,11] and the binding sites for C1q and FcγRs on the Fc domain of IgG1 show substantial overlap[12-14] (Figure 1D). We examined several amino acids at the shared IgG binding interface for C1q and FcγR that differentially modulated FcγR- and C1q binding affinity (data not shown). Mutations G236R and G237A were selected to simultaneously maximize the therapeutic index between individual and mutually dependent C1q recruitment, and to suppress or eliminate FcγR-mediated effector functions such as antibody dependent cellular cytotoxicity (ADCC) and antibody dependent cellular phagocytosis (ADCP) (Supplementary Figure 3, Figure 1C-D). Hexamerization-independent FcγR binding and activation was strongly suppressed by introducing G236R in IgG1-Campath-E430G-K439E (IgG1-Campath-RGE) and G237A in IgG1-11B8-E430G-S440K (IgG1-11B8-AGK), both for the two single agents as well as in the mixture of both components (Figure 3A, Supplementary Figure 4). In a functional assay setup, no ADCC could be detected using either of the single antibody components or the antibody combination (Figure 3B). By contrast, low level ADCP activity was still detectable, which may be attributed to residual binding to FcγRI and FcγRIIa by IgG1-11B8-AGK (Figure 3C). Importantly, tuning of the C1q binding affinity using G236R eliminated the single agent CDC activity of IgG1-Campath-RGE on Wien-133 tumor B cells, while mixed IgG1-Campath-RGE and IgG1-11B8-AGK recovered highly potent CDC activity (Figure 3D), indicating

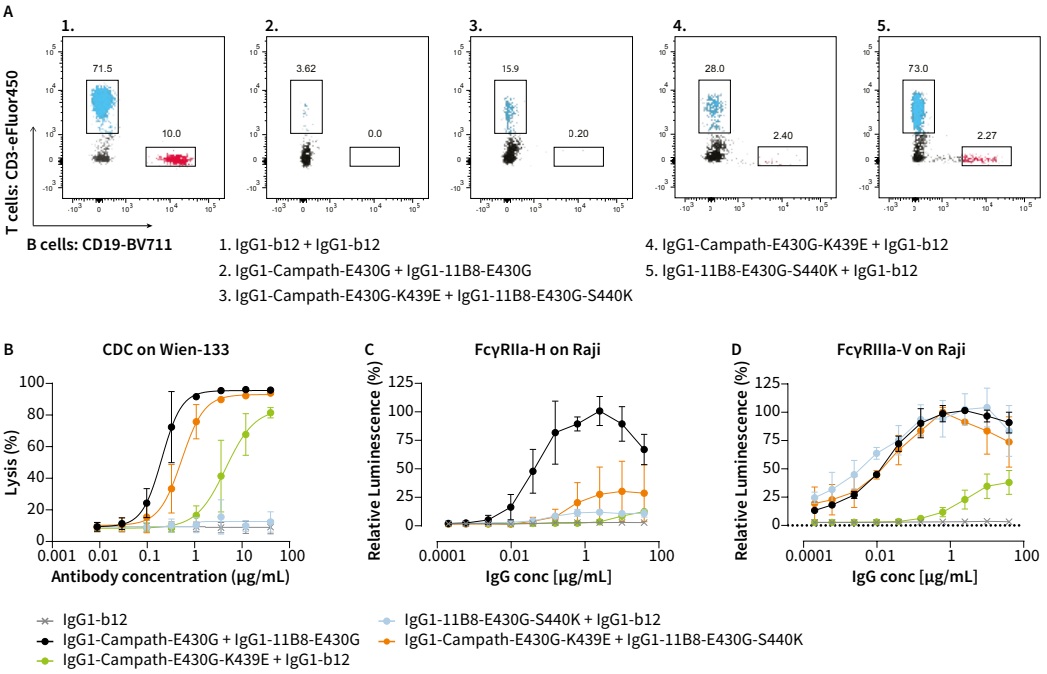

▲ **Figure 2**

Non-selective depletion of hematological cell subsets by CD52 and CD20 antibody combinations.
(**A**) B- and T-cell cytotoxicity was assessed in healthy human whole blood incubated with non-binding control antibody IgG1-b12 or equimolar mixtures (final concentration 10 µg/mL total IgG) of anti-CD52 mAb IgG1-Campath and anti-CD20 mAb IgG1-11B8 antibody variants for 18 hours at 37 °C and analyzed by flow cytometry. The fraction (%) of B- or T cells remaining within the lymphocyte population (CD66b$^-$) from one representative donor (out of 5 tested donors) is shown. (**B**) CDC of Wien-133 cells in dose-response titrations of IgG1-Campath and IgG1-11B8 antibody variants. Mean and standard deviation (SD) from three experimental repeats are shown.(**C-D**) Dose-dependent activation of FcγRIIa- (**C**) and FcγRIIIa-mediated (**D**) intracellular signaling by IgG1-Campath and IgG1-11B8 antibody variants was quantified by a luminescent reporter bioassay using Raji target cells and Jurkat T-effector cells expressing FcγRIIa H131 (**C**) or FcγRIIIa V158 (**D**). Luminescence values were normalized to the value for 10 µg/mL IgG1-11B8-E430G + IgG1-b12 prior to pooling, and are presented as the percentage relative luminescence. Mean and SD from three experimental repeats are shown. (**B-D**) Statistical analysis of area under the curve (AUC) values is described in Supplementary Table 3.

that complement activation was strictly mutually dependent. Non-equimolar target expression, as well as the asymmetric C1q binding affinity imposed by mutations G236R and G237A, restricted C1q binding by mixed IgG1-Campath-RGE and IgG1-11B8-AGK components to levels comparable to that of the wild-type IgG1-Campath and IgG1-11B8 combination (Supplementary Figure 5).

We also investigated if the selected mutations affected the pharmacokinetic profile of IgG1-Campath and IgG1-11B8 antibodies by analyzing the clearance rate in tumor free C.B-17 SCID mice in the absence of target binding. Both single IgG1-Campath-RGE and IgG1-11B8-AGK antibody components showed clearance rates comparable to those of wild-type IgG1-Campath and IgG1-11B8, respectively. Mixed IgG1-Campath-RGE and IgG1-11B8-AGK components

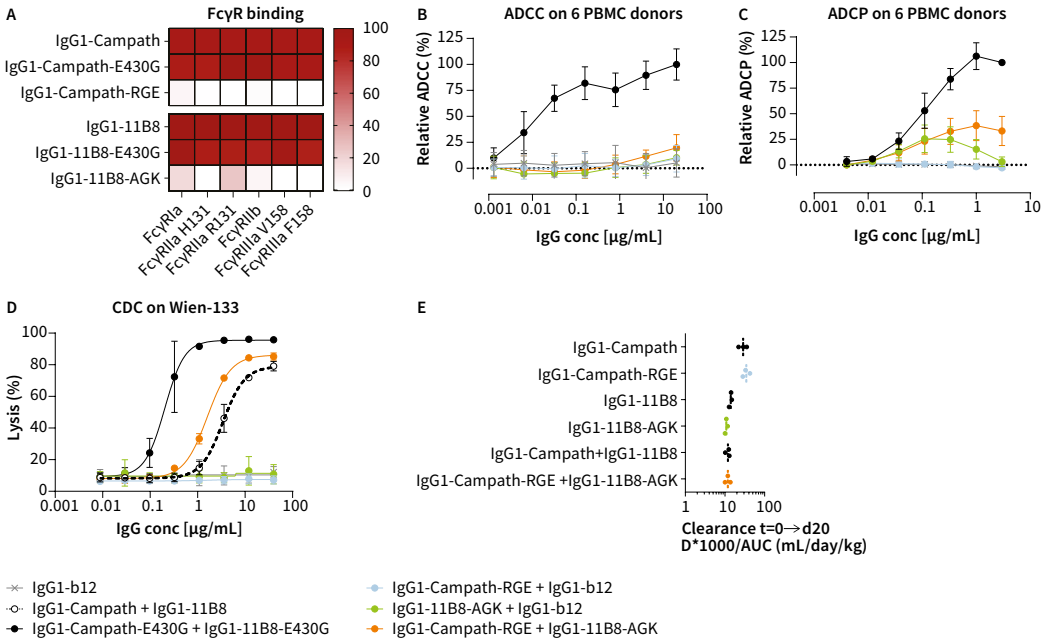

▲ **Figure 3**

Clustering-dependent effector function activation by differential modulation of effector binding through G236/G237 mutations.

(**A**) Binding of 20 µg/mL IgG1-Campath and IgG1-11B8 antibody variants to FcγRs (ELISA). Data were normalized to IgG1-b12 (0% binding) and wild-type IgG1-Campath or IgG1-11B8 (100% binding) and presented as the mean of three independent experiments. (**B**) ADCC or (**C**) ADCP by IgG1-Campath and IgG1-11B8 antibody variants using (**B**) Wien-133 target cells and PBMC effector cells (E:T 1:100), or (**C**) Calcein AM-labeled Raji target cells and CD11b^{+} h-MDM effector cells (E:T 2:1). Data were normalized to IgG1-b12 (0% ADCC/ADCP) and a mixture of IgG1-Campath-E430G and IgG1-11B8-E430G (100% ADCC/ADCP). Mean and SD of six donors are shown. (**D**) CDC of Wien-133 cells by IgG1-Campath and IgG1-11B8 antibody variants. Mean and SD from three experimental repeats are shown. (**B-D**) Statistical analysis of AUC values is described in Supplementary Table 3. (**E**) PK analysis of IgG1-Campath and IgG1-11B8 antibody variants in SCID mice (three mice per group). Clearance of a single antibody dose (500 µg) was monitored for three weeks and is expressed as Dose (D)*1,000/AUC. Statistical comparison between groups is described in Supplementary Table 4.

displayed a clearance rate similar to that of a mixture of wild type IgG1-Campath and IgG1-11B8 (Figure 3E).

A mutually dependent antibody combination induces selective depletion of healthy and tumor B cells co-expressing CD52 and CD20

To assess whether cytotoxicity of the IgG1-Campath-RGE and IgG1-11B8-AGK antibody combination is restricted to cells co-expressing CD52 and CD20, we analyzed the CDC activity of individual and mixed antibody components on six tumor B-cell lines with variable CD52 and CD20 target expression levels. All six cell lines were sensitive to CDC by a combination of the independently hexamerizing antibodies IgG1-Campath-E430G and IgG1-11B8-E430G. Tested as single components, neither IgG1-Campath-RGE, nor IgG1-11B8-AGK induced

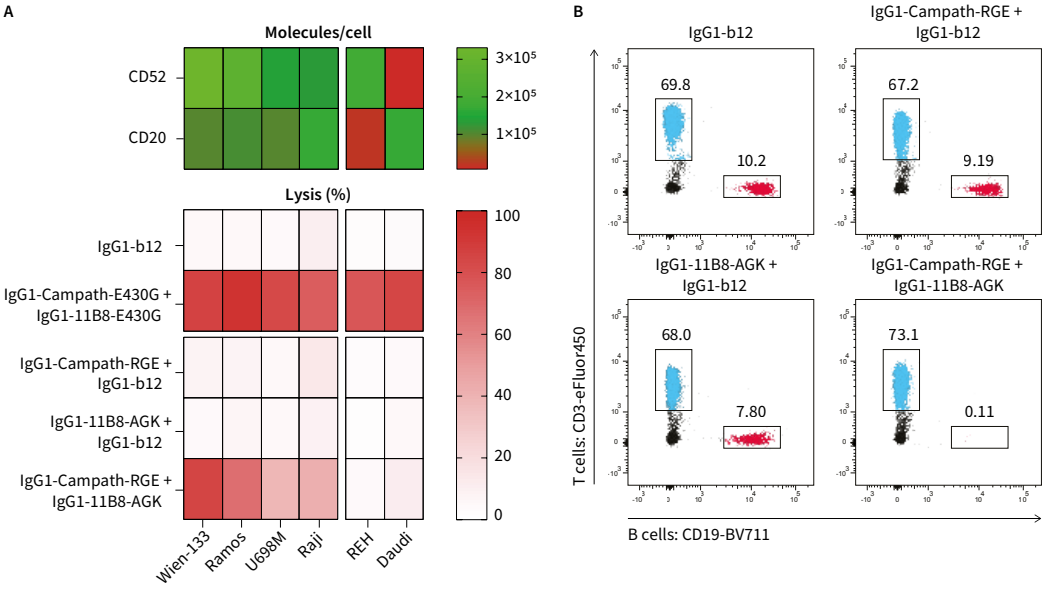

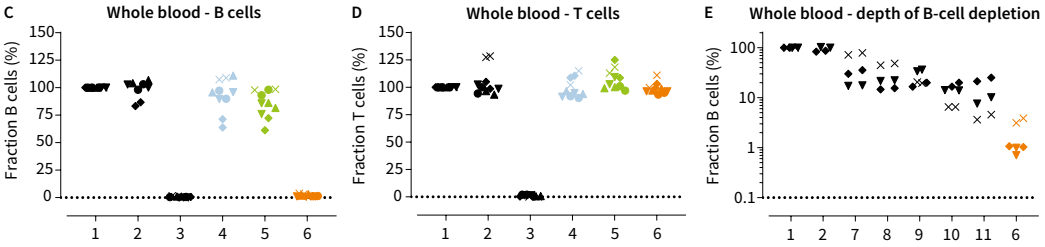

1. No Ab
2. IgG1-b12
3. IgG1-Campath-E430G + IgG1-11B8-E430G
4. IgG1-CD52-Campath-RGE + IgG1-b12
5. IgG1-11B8-AGK + IgG1-b12
6. IgG1-Campath-RGE + IgG1-11B8-AGK
7. Rituximab + IgG1-b12
8. Obinutuzumab + IgG1-b12
9. IgG1-11B8 + IgG1-b12
10. IgG1-11B8-E430G + IgG1-b12
11. IgG1-7D8 + IgG1-b12

Donor 1
Donor 2
Donor 3
Donor 4
Donor 5

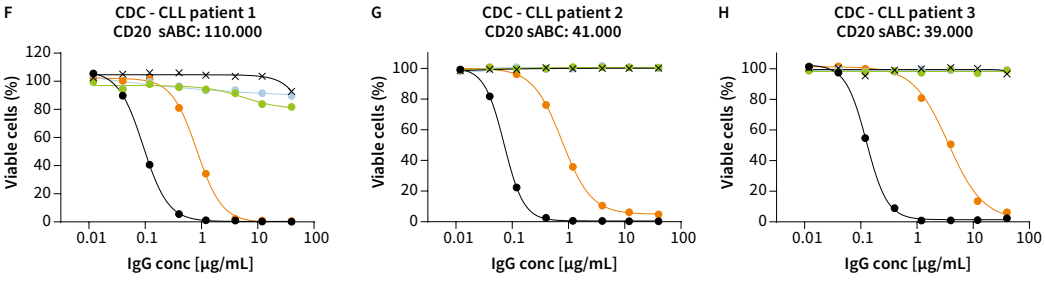

IgG1-b12
IgG1-Campath-E430G + IgG1-11B8-E430G
IgG1-Campath-RGE + IgG1-b12
IgG1-11B8-AGK + IgG1-b12
IgG1-Campath-RGE + IgG1-11B8-AGK

◀ **Figure 4**

Mutually dependent CD52 and CD20 antibody combinations induced selective depletion of healthy- and tumor B cells. (**A**) CDC (lower panel) induced by IgG1-Campath and IgG1-11B8 antibody variants (40 µg/mL final concentration) in different B-tumor cell lines expressing various levels of CD52 and CD20 quantified by the number of antibody molecules bound per cell (top panel). Data shown are mean values of at least three independent experiments. (**B-E**) Cytotoxicity induced by IgG1-Campath and IgG1-11B8 antibody variants (10 µg/mL final concentration) incubated for 18 hours in healthy human whole blood, as analyzed by flow cytometry. (**B**) The fraction (%) of B or T cells remaining within the lymphocyte population ($CD66b^-$) is shown for one representative donor. (**C-D**) Summary of cytotoxicity results relative to a non-treated (no antibody) control sample for five donors containing variable levels of B and T cells. (**E**) B-cell depletion induced by mutually dependent IgG1-Campath and IgG1-11B8 antibody combinations compared to that of different existing CD20 antibody molecules, shown for three donors relative to a non-treated (no antibody) control sample. (**F**) Dose response CDC in PBMCs derived from three CLL patients opsonized with serial dilutions of IgG1-Campath and IgG1-11B8 mutant antibody variants and ranked according to CD20 expression levels. sABC, specific antibody binding capacity.

CDC on any of the cell lines tested (Figure 4A). In contrast, the combination of IgG1-Campath-RGE and IgG1-11B8-AGK induced mutually dependent CDC on CD52/CD20 double positive cell lines only, in which the maximal lysis was dependent on the relative expression of both targets.

To test selectivity for double positive cells within a heterogeneous cell mixture, we evaluated B- and T-cell depletion by the CD52- and CD20- mutually dependent antibody combination in human whole blood. Indeed, a combination of IgG1-Campath-RGE and IgG1-11B8-AGK induced selective depletion of $CD19^+$ B cells, expressing both CD52 and CD20, in human whole blood derived from five healthy donors, while the $CD3^+$ T-cell population, expressing CD52 only, remained unaffected (Figure 4B-D). Single components IgG1-Campath-RGE or IgG1-11B8-AGK did not show any depletion of B or T cells, demonstrating that cytotoxicity was dependent on binding of both components to antigens co-expressed on the same target cell. Remarkably, as compared to CD20 antibody molecules known to deplete B cells in human whole blood[15-17], the mutually dependent IgG1-Campath-RGE and IgG1-11B8-AGK antibody combination induced superior, or at least comparable depletion of B cells in human whole blood derived from three healthy donors (Figure 4E). Together, these results demonstrate highly efficient and selective CDC-driven depletion of B cells in whole blood.

Finally, the potency of the mutually dependent CD52 and CD20 antibody combination was tested in B cells derived from peripheral blood mononuclear cells (PBMCs) of CLL patients *ex vivo*. The IgG1-Campath-RGE and IgG1-11B8-AGK antibody combination induced potent and almost complete lysis of B cells derived from three different CLL patients (Figure 4F), in contrast to the individual antibody components. Collectively, these findings confirmed potent, selective and mutually dependent functional activation by the IgG1-Campath-RGE and IgG1-11B8-AGK antibody combination.

Mutually dependent antibody combinations form hetero-hexameric complexes on co-expressing cells

Antibodies targeting CD37 and CD20 were shown to co-localize and form hetero-hexameric complexes on co-expressing cell surfaces.[8] Here, we used fluorescence resonance energy transfer (FRET) analysis to test the molecular proximity of antibody combinations targeting CD52 and CD20. Purified human B cells from healthy donors were opsonized with fluorescently labeled CD52 and CD20 antibody variants added either individually or in combinations. While wild-type CD52 and CD20 antibody combinations elicited limited proximity-induced FRET, introduction of hexamerization-enhancing mutation E430G increased FRET intensity (Figure 5A). Intriguingly, adding purified C1q or C1 enhanced FRET induction by combinations of CD52 and CD20 antibodies only if they contained mutation E430G, suggesting that Fc-Fc interactions and C1q or C1 recruitment cooperatively promoted CD52 and CD20 antibody co-localization. The mutually dependent CD52 and CD20 antibody combination IgG1-Campath-RGE and IgG1-11B8-AGK induced FRET levels similar to those of a combination of CD52 and CD20 antibodies containing an E430G mutation, whereas FRET was substantially reduced for either single antibody component (Figure 5B). Thus, hetero-hexamer formation and proximity-induced FRET by mutually dependent antibody combinations was dependent on binding of both components to the same target cell.

We next evaluated how mixing mutually dependent CD52 and CD20 antibody components at non-equimolar concentrations affected CDC potency. At saturating concentrations of either IgG1-Campath-RGE or IgG1-11B8-AGK, a titration of the second antibody component recovered essentially identical CDC activity compared to an equimolar mixture of the antibody combination, indicating that specificity and potency was preserved for a range of different mixture compositions (Figure 5C).

We also examined whether non-binding antibodies could be recruited from solution by cell surface-bound antibodies if both contain complementary mutations. Mixing either IgG1-Campath-RGE or IgG1-11B8-AGK with non-binding antibodies containing Fc domains with complementary mutations (IgG1-b12-AGK and IgG1-b12-RGE respectively) did not result in detectable CDC activity in a panel of six tumor B-cell lines (Figure 5D). This indicates that antigen binding-independent recruitment did not meaningfully contribute to tumor cell kill induced by mutually dependent antibody combinations.

For tumor targeting applications, it could be beneficial to permit ADCC activity selectively for a tumor-specific antibody component, when used in combination with a component that targets a more broadly expressed antigen. We therefore analyzed the impact of preserving FcγR binding in antibody compo-

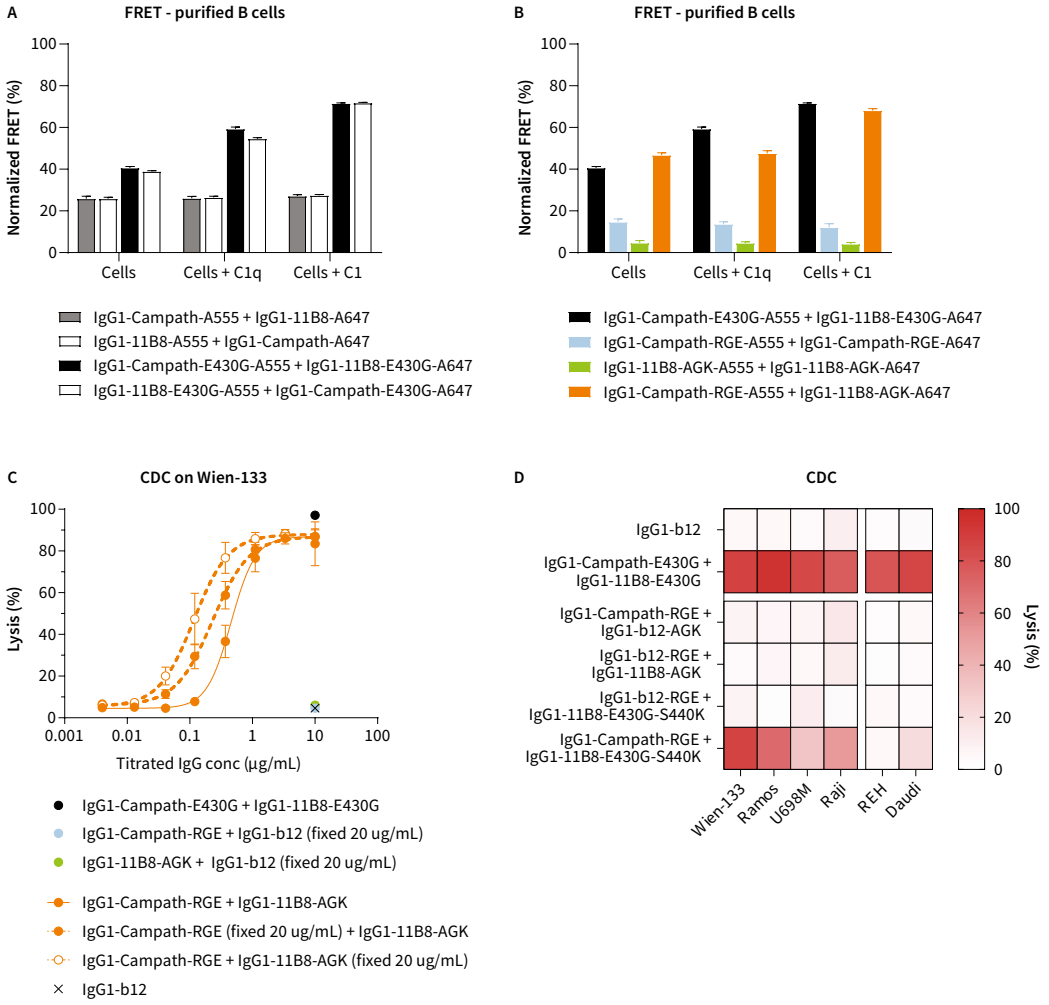

▲ Figure 5

Cell surface co-localization by mutually dependent CD52 and CD20 antibody combinations

(**A**-**B**) FRET analysis to detect the molecular proximity of (**A**) wild-type and E430G mutant IgG1-Campath or IgG1-11B8 antibody combinations or (**B**) IgG1-Campath and IgG1-11B8 mutually dependent antibody combinations. Purified healthy donor B cells were opsonized with 10 µg/mL A555-conjugated- and 10 µg/mL A647-conjugated antibody variants in the presence or absence of purified human C1q (2.5 µg/mL) or C1 (2.42 µg/mL) and FRET was calculated from normalized MFI values as determined by flow cytometry. Data shown are mean and SD of four replicates collected from two independent experiments. (**C**) Dose response CDC on Wien-133 cells opsonized with non-equimolar mixtures of mutually dependent IgG1-Campath and IgG1-11B8 antibody combinations. Titrated antibodies were mixed with antibodies at a fixed (10 µg/mL) concentration. Mean and SD from three experimental repeats are shown. See Supplementary Table 3 for statistical analysis of AUC values. (**D**) CDC induced by IgG1-Campath and IgG1-11B8 antibody variants (40 µg/mL final concentration) in different B-tumor cell lines. Data shown are mean values of at least three independent experiments.

nent IgG1-11B8-E430G-S440K (Figure 2B-D) on the CDC activity after mixing with IgG1-Campath-RGE (Figure 5D). This functionally asymmetric antibody combination retained selective activation of CDC only on CD52/CD20 double positive cell lines, while recruiting more C1q than the FcγR-suppressed antibody combination (Supplementary Figure 5). These results indicate that the effector functions of such combinations can be adapted to the target expression profiles and product design specifications.

Mutually dependent antibody combinations can target distinct cellular subsets distinguished by different antigen combinations

Potential applications of mutually dependent antibody combinations composed of one antibody with RGE mutations and one antibody with AGK mutations were further explored for different target combinations. A combination of antibodies targeting CD37 (IgG1-CD37.3-RGE) and CD20 (IgG1-11B8-AGK) induced potent and mutually dependent CDC on a CD37 and CD20 double-positive tumor cell line (Figure 6A). We next investigated whether, in addition to B-cells, also other cellular subsets could be selectively targeted using antibody combinations. We therefore tested if T cells could be selectively depleted in human whole blood using an antibody combination targeting CD52 (IgG1-Campath-RGE) and CD3 (IgG1-huCLB3/4-AGK), which are co-expressed on T cells. Indeed, the antibody combination targeting CD52 and CD3 induced selective depletion of $CD4^+$ T cells expressing both CD52 and CD3, while sparing CD52-only expressing B cells in human whole blood derived from four healthy donors (Figure 6B). T-cell depletion was strictly mutually dependent, as neither of the single antibody components induced any T- or B-cell depletion.

We thus far showed that mutually dependent antibody combinations could regulate hexamerization-dependent complement activation. Hexamerization-enhanced antibodies targeting TNFR superfamily members such as death receptor 5 (DR5) and OX40, which are activated via higher order receptor clustering, were also reported to enhance agonistic signaling and tumor cell death (Supplementary Figure 6)[3,6]. Hence, we evaluated whether an antibody combination targeting non-overlapping epitopes on DR5 (IgG1-DR5-01-RGE and IgG1-DR5-05-AGK) could achieve agonistic activation. Indeed, while both single antibody components were silent, the antibody combination targeting DR5 showed potent induction of apoptosis in COLO-205 and Bx-PC3 solid tumor cell lines (Figure 6C). In contrast, dual epitope targeting by the two WT antibodies showed limited to no efficacy (Supplementary Figure 6). Collectively, these results illustrate that mutually dependent antibody combinations can be designed to target different cell surface antigen combinations, and to elicit potent complement activation or agonistic activation of target signaling[3].

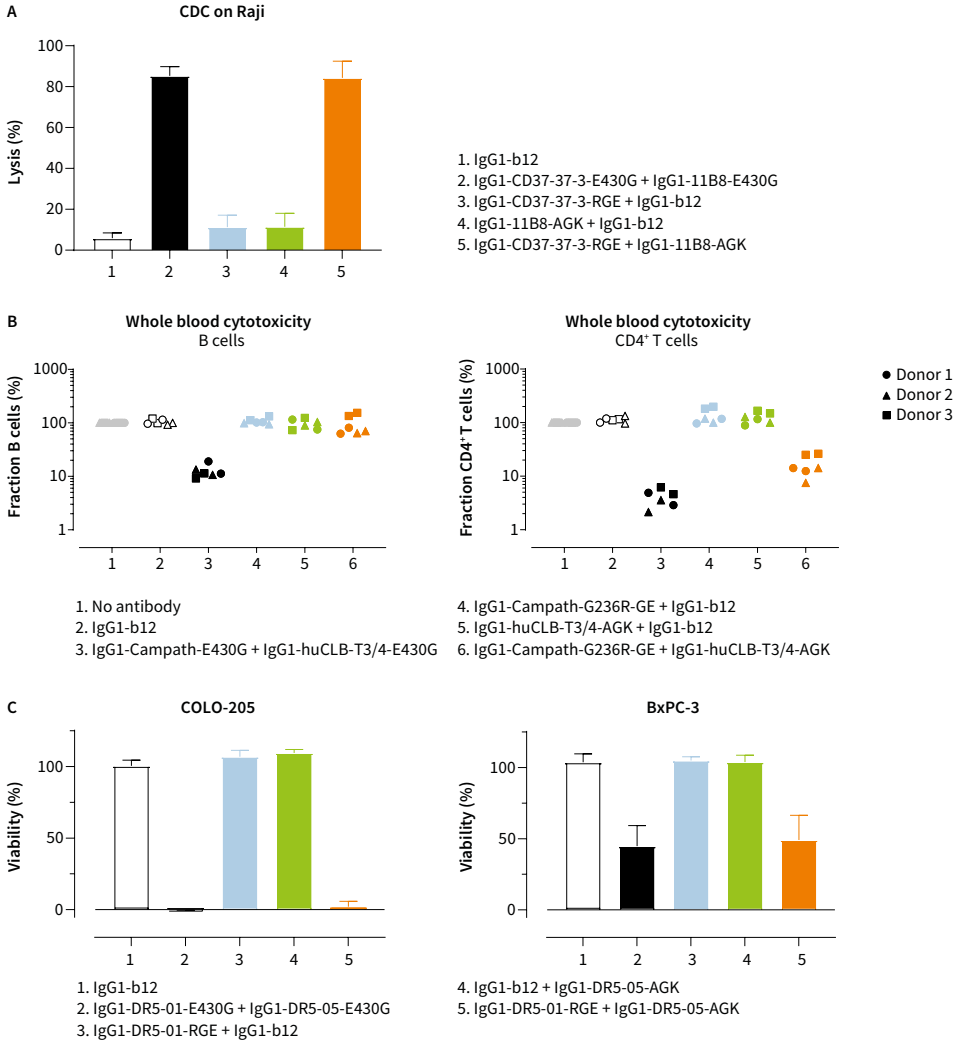

▲ **Figure 6**

Mutually dependent antibody combinations are applicable to different cell surface antigen combinations.
(**A**) CDC on Raji cells opsonized with 40 µg/mL anti-CD37 mAb IgG1-37.3 and IgG1-11B8 antibody variants. Mean and SD from three independent experiments are shown. See Supplementary Table 3 for statistical analysis of AUC values. (**B**) Cytotoxicity induced by anti-CD3 mAb IgG1-huCLB-T3/4 and IgG1-Campath antibody variants (10 µg/mL final concentration) incubated for 45 minutes in healthy human whole blood, as analyzed by flow cytometry. The fraction (%) of B cells and $CD4^+$ T cells remaining within the lymphocyte population ($CD66b^-$) is shown for three individual donors relative to a non-treated (no antibody) control sample. (**C**) COLO-205 and BxPC-3 cells were incubated with anti-DR5 IgG1-DR5-01 and IgG1-DR5-05 antibody variants (final concentration 20 µg/mL) in the presence of 2.5 µg/mL purified human C1q and cell viability (%) was measured after 72 hours. Mean ± SD of data from three independent experiments are shown. See Supplementary Table 3 for statistical analysis of AUC values.

DISCUSSION

Activation of antibody-mediated effector functions to eliminate pathogens or destroy tumor cells primarily requires avid antibody binding to cognate antigens on the target cell. Potent effector activity by antibody-based therapies however, may lead to undesired on- or off-target toxicity[18]. Here, we describe an AND-gated approach to decouple effector function activation by antibody combinations from individual antibody binding events. Both antibodies may target different membrane receptors and bind various cellular subtypes individually, but specific point mutation combinations modulate Fc-Fc, C1q and Fc gamma receptor (FcγR) interactionsto make IgG hetero-oligomerization and functional activation stringently dependent on the presence of both antibody components[2,7,8,19]. This AND-gated approach was generalizable to different effector mechanisms, including complement activation and agonistic signaling, and to multiple target combinations present on both hematologic and solid tumor cells. Asymmetric silencing of FcγR-mediated effector functions in antibody combinations was possible, enabling design variations that mitigate or leverage on-target toxicity depending on target expression profiles. In some assays, the G237A mutation appeared to only partially suppress FcγR binding and ADCP activity consistent with recent findings[20], which may limit its application when targeting some broadly and highly expressed antigens, although full selectivity was preserved in whole blood assays in the presence of PBMC populations.

Potential therapeutic applications of mutually dependent antibody combinations requires targets that co-localize and/or allow for antibody hetero-hexamerization after target binding. This process may be affected by target-specific restraints other than abundance, such as antigen size, density, mobility, epitope-membrane distance, surface distribution, and the compatibility of epitopes with antibody hetero-hexamer formation[10,21-25]. The challenge of identifying target and epitope combinations that recover maximal potency seems reminiscent of the challenges inherent to covalent bispecific antibody design[26]. Nevertheless, an AND-gated approach could considerably broaden the therapeutic combinatorial target space and thereby simultaneously enhance the therapeutic index. For example, highly potent but “toxic” activity of antibodies directed towards broadly expressed, non-tumor-specific targets could be made dependent on the presence of antibodies directed against disease-specific targets. Herein, we consistently observed that mutually dependent antibody pairs retained maximal potency at doses exceeding target saturation, while avoiding the potency loss referred to as the hook or prozone effect, caused by the self-competition observed for covalent bispecific

designs[27]. This is explained by the strict dependence of antibody hexamerization and C1q binding on prior cell surface antigen binding, while monomeric antibodies in solution are incapable of C1q binding. Appropriate dosing might theoretically represent another challenge in the design of mutually dependent antibody combinations, as both components in the mixture might show different pharmacokinetics. Experiments with a wide range of non-equimolar antibody concentrations retained consistent potency, suggesting that non-equimolar mixtures could provide an option to address differences in clearance rates of the two components.

Artificial logic gates, inspired by electronic engineering, have been applied in synthetic biology to control biological processes[28-30]. In human disease, Boolean logic gates are increasingly examined for their potential to enhance therapeutic selectivity, in particular for improving the specificity of natural, or chimeric antigen receptor (CAR), T-cell recruitment[31-35]. In another approach, Boolean logic was applied to create auto-inhibited or capped AND-gated antibodies that rely on a second, exogenous factor to activate binding[36]. The AND-gated approach we describe here solely decouples antibody binding from effector function activation to achieve selectivity and is therefore not dependent on the environmental presence of secondary molecules such as enzymes or proteases. The mutually dependent antibody combinations described herein are minimally engineered, displayed regular pharmacokinetic properties, and preserved regular manufacturability and developability characteristics. We therefore expect this approach to be broadly applicable to IgG Fc-domain based therapeutics, and generalizable to multiple applications, including direct cell killing, agonistic activation, and potentially other more complex Boolean logic gates. Furthermore, the methodology described herein is readily applicable to combinatorial, high throughput screening of large antibody panels for drug discovery. As for any therapeutic, potential novel drug candidates based on AND-gated IgG backbones will require careful assessment of efficacy, safety, and different manufacturing and dosing strategies.

In summary, we present an approach to generate mutually dependent antibody combinations (HexElect) that only allow for pairwise hetero-hexamerization and effector function activation after binding to two targets co-expressed at the same cell surface. This decoupling of effector function activation from individual antibody binding events provides a unique opportunity to enhance selectivity while maintaining potency, and may allow for the creation of a next generation of differentiated antibody therapeutics.

REFERENCES

1. Wang X, Mathieu M, Brezski RJ. IgG Fc engineering to modulate antibody effector functions. *Protein Cell* 2018; **9**(1): 63-73.

2. Diebolder CA, Beurskens FJ, de Jong RN, et al. Complement is activated by IgG hexamers assembled at the cell surface. *Science* 2014; **343**(6176): 1260-3.

3. Overdijk MB, Strumane K, Beurskens FJ, et al. Dual epitope targeting and enhanced hexamerization by DR5 antibodies as a novel approach to induce potent anti-tumor activity through DR5 agonism. *Mol Cancer Ther* 2020: molcanther.0044.2020.

4. Strasser J, de Jong RN, Beurskens FJ, et al. Unraveling the Macromolecular Pathways of IgG Oligomerization and Complement Activation on Antigenic Surfaces. *Nano lett* 2019; **19**(7): 4787-96.

5. Ugurlar D, Howes SC, de Kreuk BJ, et al. Structures of C1-IgG1 provide insights into how danger pattern recognition activates complement. *Science* 2018; **359**(6377): 794-7.

6. Zhang D, Goldberg MV, Chiu ML. Fc Engineering Approaches to Enhance the Agonism and Effector Functions of an Anti-OX40 Antibody. *J Biol Chem* 2016; **291**(53): 27134-46.

7. de Jong RN, Beurskens FJ, Verploegen S, et al. A Novel Platform for the Potentiation of Therapeutic Antibodies Based on Antigen-Dependent Formation of IgG Hexamers at the Cell Surface. *PLOS Biol* 2016; **14**(1): e1002344.

8. Oostindie SC, van der Horst HJ, Lindorfer MA, et al. CD20 and CD37 antibodies synergize to activate complement by Fc-mediated clustering. *Haematologica* 2019.

9. Rao SP, Sancho J, Campos-Rivera J, et al. Human Peripheral Blood Mononuclear Cells Exhibit Heterogeneous CD52 Expression Levels and Show Differential Sensitivity to Alemtuzumab Mediated Cytolysis. *PLoS One* 2012; **7**(6): e39416.

10. Teeling JL, Mackus WJ, Wiegman LJ, et al. The biological activity of human CD20 monoclonal antibodies is linked to unique epitopes on CD20. *J Immunol* 2006; **177**(1): 362-71.

11. Wang G, de Jong RN, van den Bremer ET, et al. Molecular Basis of Assembly and Activation of Complement Component C1 in Complex with Immunoglobulin G1 and Antigen. *Mol Cell* 2016; **63**(1): 135-45.

12. Idusogie EE, Presta LG, Gazzano-Santoro H, et al. Mapping of the C1q binding site on rituxan, a chimeric antibody with a human IgG1 Fc. *J Immunol* 2000; **164**(8): 4178-84.

13. Morgan A, Jones ND, Nesbitt AM, Chaplin L, Bodmer MW, Emtage JS. The N-terminal end of the CH2 domain of chimeric human IgG1 anti-HLA-DR is necessary for C1q, Fc gamma RI and Fc gamma RIII binding. *Immunology* 1995; **86**(2): 319-24.

14. Shields RL, Namenuk AK, Hong K, et al. High resolution mapping of the binding site on human IgG1 for Fc gamma RI, Fc gamma RII, Fc gamma RIII, and FcRn and design of IgG1 variants with improved binding to the Fc gamma R. *J Biol Chem* 2001; **276**(9): 6591-604.

15. Bologna L, Gotti E, Manganini M, et al. Mechanism of Action of Type II, Glycoengineered, Anti-CD20 Monoclonal Antibody GA101 in B-Chronic Lymphocytic Leukemia Whole Blood Assays in Comparison with Rituximab and Alemtuzumab. *J Immunol* 2011; **186**(6): 3762.

16. van Meerten T, Rozemuller H, Hol S, et al. HuMab-7D8, a monoclonal antibody directed against the membrane-proximal small loop epitope of CD20 can effectively eliminate CD20 low expressing tumor cells that resist rituximab-mediated lysis. *Haematologica* 2010; **95**(12): 2063-71.

17. Bologna L, Gotti E, Da Roit F, et al. Ofatumumab Is More Efficient than Rituximab in Lysing B Chronic Lymphocytic Leukemia Cells in Whole Blood and in Combination with Chemotherapy. *J Immunol* 2013; **190**(1): 231.

18. Alinari L, Lapalombella R, Andritsos L, Baiocchi RA, Lin TS, Byrd JC. Alemtuzumab (Campath-1H) in the treatment of chronic lymphocytic leukemia. *Oncogene* 2007; **26**(25): 3644-53.

19. Hezareh M, Hessell AJ, Jensen RC, van de Winkel JG, Parren PW. Effector function activities of a panel of mutants of a broadly neutralizing antibody against human immunodeficiency virus type 1. *J Virol* 2001; **75**(24): 12161-8.

20. Brinkhaus M, Douwes RGJ, Bentlage AEH, et al. Glycine 236 in the Lower Hinge Region of Human IgG1 Differentiates FcγR from Complement Effector Function. *J Immunol* 2020.

21. Cragg MS, Morgan SM, Chan HT, et al. Complement-mediated lysis by anti-CD20 mAb correlates with segregation into lipid rafts. *Blood* 2003; **101**(3): 1045-52.

22. Hughes-Jones NC, Gorick BD, Howard JC, Feinstein A. Antibody density on rat red cells determines the rate of activation of the complement component C1. *Eur J Immunol* 1985; **15**(10): 976-80.

23. Parce JW, Kelley D, Heinzelmann K. Measurement of antibody-dependent binding, proteolysis, and turnover of C1s on liposomal antigens localizes the fluidity-dependent step in C1 activation. *Biochim Biophys Acta* 1983; **736**(1): 92-8.

24. Rougé L, Chiang N, Steffek M, et al. Structure of CD20 in complex with the therapeutic monoclonal antibody rituximab. *Science* 2020: eaaz9356.

25. Xia MQ, Hale G, Waldmann H. Efficient complement-mediated lysis of cells containing the CAMPATH-1 (CDw52) antigen. *Mol Immunol* 1993; **30**(12): 1089-96.

26. Labrijn AF, Janmaat ML, Reichert JM, Parren P. Bispecific antibodies: a mechanistic review of the pipeline. *Nat Rev Drug Discov* 2019; **18**(8): 585-608.

27. Mazor Y, Yang C, Borrok MJ, et al. Enhancement of Immune Effector Functions by Modulating IgG's Intrinsic Affinity for Target Antigen. *PLoS One* 2016; **11**(6): e0157788-e.

28. Hasty J, McMillen D, Collins JJ. Engineered gene circuits. *Nature* 2002; **420**(6912): 224-30.

29. Lu TK, Khalil AS, Collins JJ. Next-generation synthetic gene networks. *Nat Biotechnol* 2009; **27**(12): 1139-50.

30. Chen Z, Kibler RD, Hunt A, et al. De novo design of protein logic gates. *Science* 2020; **368**(6486): 78.

31. Lajoie MJ, Boyken SE, Salter AI, et al. Designed protein logic to target cells with precise combinations of surface antigens. *Science* 2020; **369**(6511): 1637.

32. Minogue E, Millar D, Chuan Y, et al. Redirecting T-Cells Against AML in a Multidimensional Targeting Space Using T-Cell Engaging Antibody Circuits (TEAC). *Blood* 2019; **134**(Supplement_1): 2653-.

33. Morsut L, Roybal Kole T, Xiong X, et al. Engineering Customized Cell Sensing and Response Behaviors Using Synthetic Notch Receptors. *Cell* 2016; **164**(4): 780-91.

34. Roybal Kole T, Rupp Levi J, Morsut L, et al. Precision Tumor Recognition by T Cells With Combinatorial Antigen-Sensing Circuits. *Cell* 2016; **164**(4): 770-9.

35. Banaszek A, Bumm TGP, Nowotny B, et al. On-target restoration of a split T cell-engaging antibody for precision immunotherapy. *Nat Commun* 2019; **10**(1): 5387.

36. Gunnoo SB, Finney HM, Baker TS, Lawson AD, Anthony DC, Davis BG. Creation of a gated antibody as a conditionally functional synthetic protein. *Nat Commun* 2014; **5**(1): 4388.

37. Crowe JS, Hall VS, Smith MA, Cooper HJ, Tite JP. Humanized monoclonal antibody CAMPATH-1H: myeloma cell expression of genomic constructs, nucleotide sequence of cDNA constructs and comparison of effector mechanisms of myeloma and Chinese hamster ovary cell-derived material. *Clin Exp Immunol* 1992; **87**(1): 105-10.

38. Teeling JL, French RR, Cragg MS, et al. Characterization of new human CD20 monoclonal antibodies with potent cytolytic activity against non-Hodgkin lymphomas. *Blood* 2004; **104**(6): 1793-800.

39. Maloney DG, Liles TM, Czerwinski DK, et al. Phase I clinical trial using escalating single-dose infusion of chimeric anti-CD20 monoclonal antibody (IDEC-C2B8) in patients with recurrent B-cell lymphoma. *Blood* 1994; **84**(8): 2457-66.

40. Mossner E, Brunker P, Moser S, et al. Increasing the efficacy of CD20 antibody therapy through the engineering of a new type II anti-CD20 antibody with enhanced direct and immune effector cell-mediated B-cell cytotoxicity. *Blood* 2010; **115**(22): 4393-402.

41. Parren PW, Geerts ME, Boeije LC, Aarden LA. Induction of T-cell proliferation by recombinant mouse and chimeric mouse/human anti-CD3 monoclonal antibodies. *Res Immunol* 1991; **142**(9): 749-63.

42. Deckert. J. CD37-binding molecules and immunoconjugates thereof. *WO 2011/112978A1* 2011.

43. Burton DR, Pyati J, Koduri R, et al. Efficient neutralization of primary isolates of HIV-1 by a recombinant human monoclonal antibody. *Science* 1994; **266**(5187): 1024-7.

44. Wines BD, Vanderven HA, Esparon SE, Kristensen AB, Kent SJ, Hogarth PM. Dimeric FcγR Ectodomains as Probes of the Fc Receptor Function of Anti-Influenza Virus IgG. *J Immunol* 2016; **197**(4): 1507-16.

45. Oostindie SC, van der Horst HJ, Kil LP, et al. DuoHexaBody-CD37®, a novel biparatopic CD37 antibody with enhanced Fc-mediated hexamerization as a potential therapy for B-cell malignancies. *Blood Cancer J* 2020; **10**(3): 30.

46. Saphire EO, Parren PW, Pantophlet R, et al. Crystal structure of a neutralizing human IGG against HIV-1: a template for vaccine design. *Science* 2001; **293**(5532): 1155-9.

SUPPLEMENTARY FIGURES AND TABLES

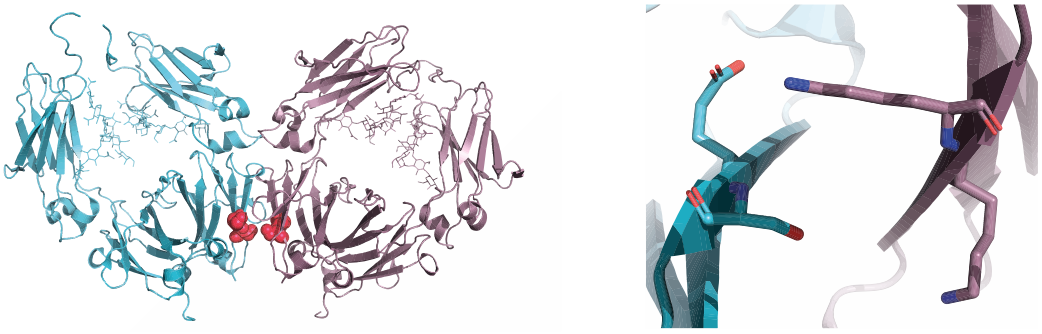

▲ **Supplementary Figure 1**

Fc-Fc interaction interface model.

Left: Ribbon diagram of two Fc segments with residues (Lys^{439} and Ser^{440}) critical for Fc-Fc interactions indicated in pink. Right: modeled interactions of a K439E (Lys^{439} → Glu) mutant facing the S440K (Ser^{440} → Lys) mutant on the complementary Fc segment of a neighboring antibody. Figure adapted from Diebolder et al. Science 343:1260-1263 (2014).

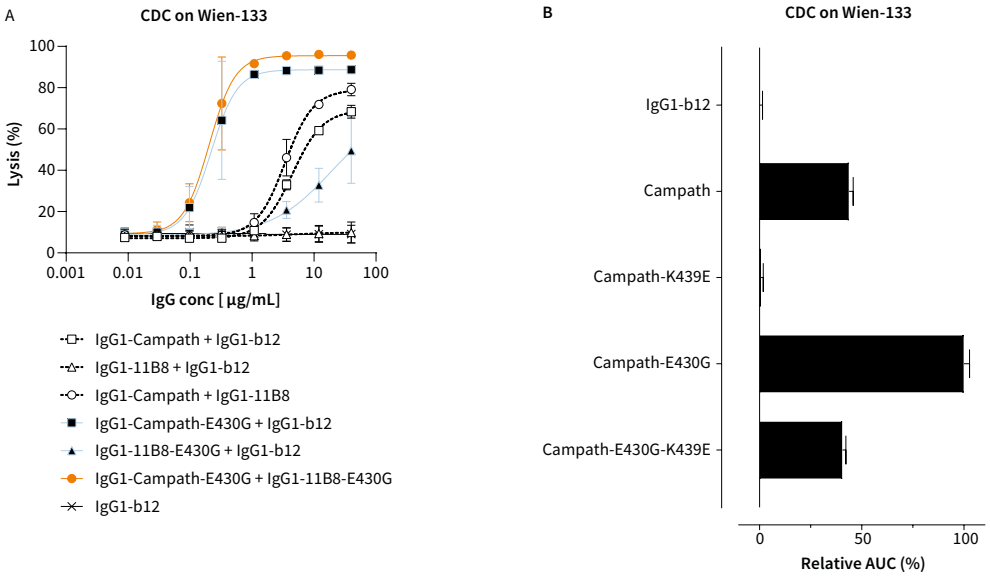

▲ **Supplementary Figure 2**

Complement-mediated cytotoxicity on Wien-133 cells opsonized with different IgG1-Campath and IgG1-11B8 antibody variants.

(**A**) CDC by wild-type and hexamerization-enhanced variants of CD52 and CD20 antibodies. Mean and standard deviation (SD) from three experimental repeats are shown. (**B**) Residual CDC by Fc-Fc interface mutant CD52 antibody variants. CDC was assessed on Wien-133 cells opsonized with a concentration series of different IgG1-Campath antibody variants. Data was averaged over three experiments, normalized to IgG1-b12 (0 % lysis) and IgG1-Campath-E430G (100% lysis), and is presented as the area under the curve (AUC). (**A-B**) See Supplementary Table 3 for statistical analysis of AUC values.

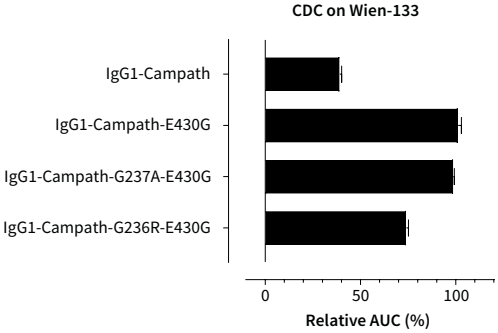

▲ **Supplementary Figure 3**

Complement activation by C1q- and FcγR-binding mutant CD52 antibody variants.

CDC was assessed using Wien-133 cells opsonized with a concentration series of different IgG1-Campath antibody variants. Data was averaged over three experiments, normalized to IgG1-b12 (0 % lysis) and IgG1-Campath-E430G (100% lysis), and is presented as the area under the curve (AUC). See Supplementary Table 3 for statistical analysis of AUC values.

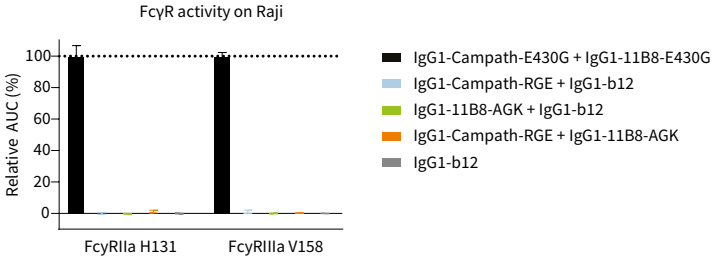

▲ Supplementary Figure 4

Activation of FcγRIIa- and FcγRIIIa-mediated intracellular signaling by IgG1-Campath and IgG1-11B8 mutant antibody variants.

Activation of FcγR-mediated signaling was assessed in a Luminescent Reporter Bioassay using Raji target cells and Jurkat T-effector cells. Luminescence values were normalized to the value of 10 µg/mL IgG1-11B8-E430G + IgG1-b12 prior to pooling. Area under the curve (AUC) values were averaged over three experiments, normalized to IgG1-b12 (0 % activation) and a mixture of IgG1-11B8-E430G and IgG1-Campath-E430G (100% activation). See Supplementary Table 3 for statistical analysis of AUC values.

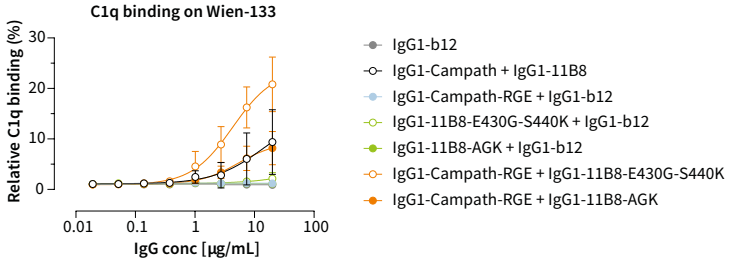

▲ Supplementary Figure 5

C1q binding by IgG1-Campath and IgG1-11B8 mutant antibody variants.

C1q binding to Wien-133 cells opsonized with a concentration series of IgG1-Campath and IgG1-11B8 mutant antibody variants. Data were normalized to IgG1-b12 (0 % C1q binding) and a mixture of IgG1-11B8-E430G and IgG1-Campath-E430G (100% C1q binding). Mean and standard deviation (SD) from three independent experiments are shown. See Supplementary Table 3 for statistical analysis of AUC values.

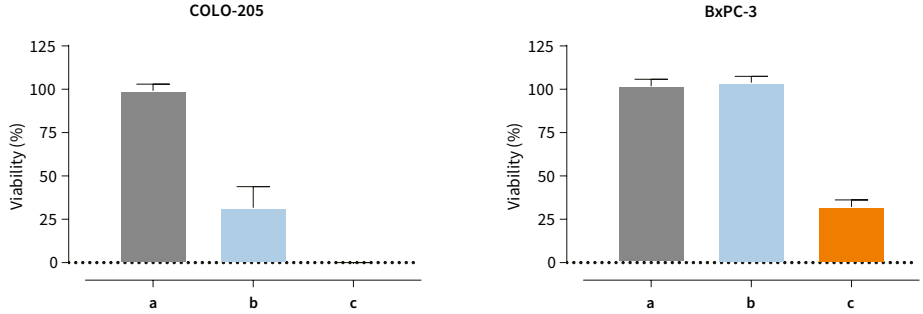

▲ Supplementary Figure 6

Agonistic activity by wild-type and hexamerization-enhanced IgG1-DR5 antibody variants.

COLO-205 and BxPC-3 cells were incubated with wild-type and hexamerization-enhanced (E430G) anti-DR5 IgG1-DR5-01 and IgG1-DR5-05 antibody variants (final concentration 20 µg/mL) in the presence of 2.5 µg/mL purifed human C1q and cell viability (%) was measured after 72 hours. Mean ± SD of data from three independent experiments are shown. See Supplementary Table 3 for statistical analysis of AUC values.

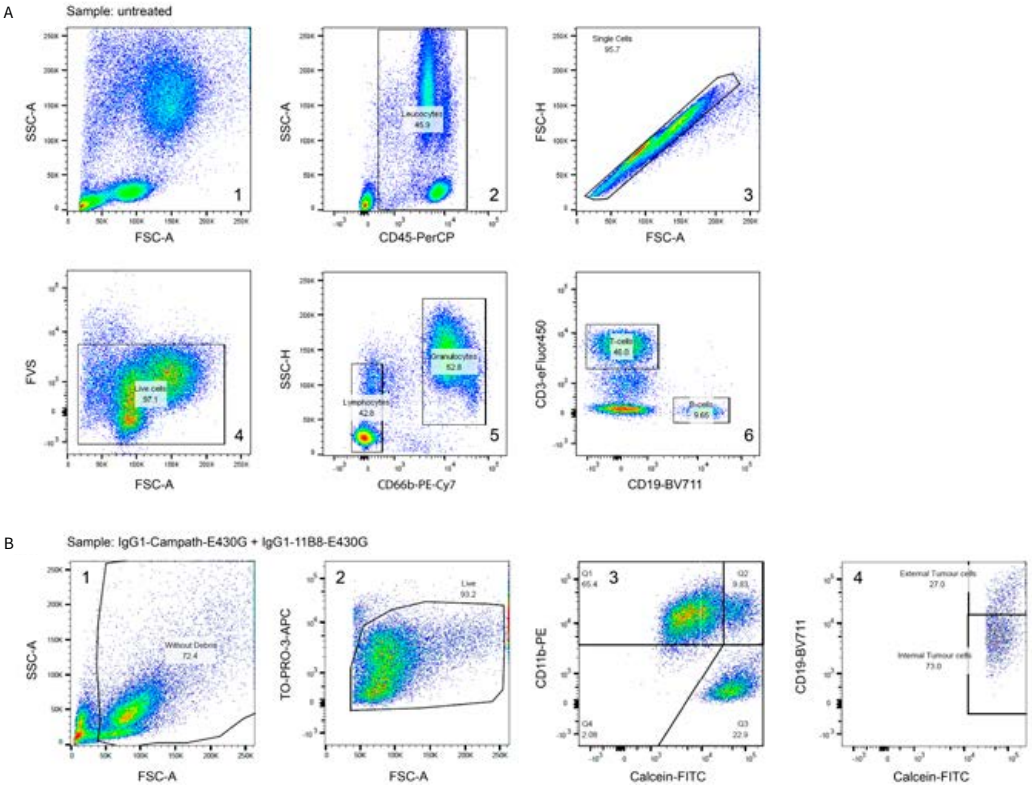

▲ Supplementary Figure 7

Flow cytometry gating strategy used to define cell populations by flow cytometry.

(**A**) Example of whole blood cytotoxicity flow cytometry gating strategy, as illustrated for a negative control sample (untreated cells) derived from a healthy human donor. (1) Cells were identified based on forward scatter (FSC) vs. side scatter (SSC). (2) Leukocytes were selected by $CD45^+$ staining. (3) Doublets were excluded by FSC-A vs. FSC-H. (4) Dead cells were excluded by TO-PRO-3 staining. (5) Lymphocytes and granulocytes were separated based on CD66b staining. (6) B- and T cells within the lymphocyte ($CD66b^-$) cell population were identified as $CD19^+$ and $CD3^+$/($CD4^+$, data not shown), respectively. Cytotoxicity was calculated as the fraction (%) of cells remaining after treatment relative to a non-treated control sample (100%). (**B**) Example of ADCP flow cytometry gating strategy, as illustrated for a positive control sample (IgG1-Campath-E430G + IgG1-11B8-E430G) with Raji target cells and human monocyte-derived macrophage (h-MDM) effector cells. (1) Cells were identified based on forward scatter (FSC) vs. side scatter (SSC). (2) Dead cells were excluded by fixable viability stain (FVS). (3) Raji target cells and h-MDM effector cells were separated by calcein AM and CD11b staining respectively. (4) CD19 was used as a marker to exclude external (non-phagocytosed) Raji target cells. $CD11b^+$/calcein AM^+/$CD19^-$ cells were identified as h-MDM that phagocytosed Daudi cells. ADCP was calculated as the fraction of $CD11b^+$/calcein AM^+/$CD19^-$ cells within the total h-MDM ($CD11b^+$) cell population.

Supplementary Table 1

Antibodies used for h-MDM characterization

Target	Label	Target expression	Company	Clone	Cat. No.
CD14	PE-Cy7	Maturation and lineage marker for monocytes/macrophages	BD Pharmingen	M5E2	557742
CD11b	PE	General myeloid cell lineage and maturation marker	BD Pharmingen	ICRF44	555388
CD64	FITC	FcγRI (IgG1), expressed on mature antigen-presenting cells including macrophages	Biolegend	10.1	305006
CD80	APC	B7-1, expressed on activated antigen-presenting cells, including macrophages	Miltenyi	2D10	130-097-204
CD163	BV421	Macrophage sub lineage/maturity marker	Biolegend	GHI/61	333612
CD206	BV711	Mannose receptor, macrophage maturity/ sub lineage marker	Biolegend	15-2	321136
FVS	eFluor660	Staining of dead cells	BD Biosciences		565694

Supplementary Table 2

Antibodies used for identification of cell subsets in ADCP assays

Target	Label	Target expression	Company	Clone	Cat. No.
CD11b	PE	h-MDM	BD Pharmingen	ICRF44	555388
CD19	BV711	Tumor B cells (Daudi)	Biolegend	SJ25C1	363026
TO-PRO-3	APC	Staining of dead cells	Molecular Probes		T3605

Supplementary Table 3

Area under the curve statistics as determined for multiple dose-response analyses

Fig.	Sub	Item[1]	Antibody component 1	Antibody component 2	Assay	Cells	N[2]	Mean rel. AUC (%)[3]	SD	95% CI of diff. to PC[4]	Adjusted P-value[5]	95% CI of diff. to NC[6]	Adjusted P-value[7]
2	b	PC	IgG1-Campath-E430G	IgG1-11B8-E430G	CDC	Wien-133	3	100.0	4.63			-107.0 to -92.98	<0.0001
2	b	TI	IgG1-Campath-E430G-K439E	IgG1-b12	CDC	Wien-133	3	34.85	5.13	57.22 to 73.09	<0.0001	-41.87 to -27.82	<0.0001
2	b	TI	IgG1-11B8-E430G-S440K	IgG1-b12	CDC	Wien-133	3	2.54	2.75	89.53 to 105.4	<0.0001	-9.566 to 4.483	0.7404
2	b	TI	IgG1-Campath-E430G-K439E	IgG1-11B8-E430G-S440K	CDC	Wien-133	3	79.85	4.05	12.22 to 28.08	<0.0001	-86.88 to -72.83	<0.0001
2	b	NC	IgG1-b12	IgG1-b12	CDC	Wien-133	6	0.00	1.87	93.13 to 106.9	<0.0001		
2	c	PC	IgG1-Campath-E430G	IgG1-11B8-E430G	FcγRIIa H131 activity	Raji	3	99.99	6.71			-110.3 to -89.67	<0.0001
2	c	TI	IgG1-Campath-E430G-K439E	IgG1-b12	FcγRIIa H131 activity	Raji	3	2.46	0.48	87.21 to 107.8	<0.0001	-12.78 to 7.856	0.8932
2	c	TI	IgG1-11B8-E430G-S440K	IgG1-b12	FcγRIIa H131 activity	Raji	3	9.01	0.98	80.66 to 101.3	<0.0001	-19.33 to 1.302	0.0904
2	c	TI	IgG1-Campath-E430G-K439E	IgG1-11B8-E430G-S440K	FcγRIIa H131 activity	Raji	2	19.87	7.01	69.80 to 90.44	<0.0001	-30.19 to -9.555	0.0008
2	c	NC	IgG1-b12	IgG1-b12	FcγRIIa H131 activity	Raji	3	0.00	0.30	89.67 to 110.3	<0.0001		
2	d	PC	IgG1-Campath-E430G	IgG1-11B8-E430G	FcγRIIIa V158 activity	Raji	3	99.99	2.33			-107.7 to -92.29	<0.0001
2	d	TI	IgG1-Campath-E430G-K439E	IgG1-b12	FcγRIIIa V158 activity	Raji	3	14.13	2.00	75.50 to 96.22	<0.0001	-21.84 to -6.428	0.0014
2	d	TI	IgG1-11B8-E430G-S440K	IgG1-b12	FcγRIIIa V158 activity	Raji	3	110.50	5.14	-20.87 to -0.1465	0.0468	-118.2 to -102.8	<0.0001
2	d	TI	IgG1-Campath-E430G-K439E	IgG1-11B8-E430G-S440K	FcγRIIIa V158 activity	Raji	2	94.10	4.45	-2.721 to 14.51	0.2079	-102.7 to -85.49	<0.0001
2	d	NC	IgG1-b12	IgG1-b12	FcγRIIIa V158 activity	Raji	3	0.00	0.17	92.29 to 107.7	<0.0001		
3	b	PC	IgG1-Campath-E430G	IgG1-11B8-E430G	ADCC	Wien-133	6	100.0	18.03			-117.9 to -82.06	<0.0001

Fig.	Sub	Item[1]	Antibody component 1	Antibody component 2	Assay	Cells	N[2]	Mean rel. AUC (%)[3]	SD	95% CI of diff. to PC[4]	Adjusted P-value[5]	95% CI of diff. to NC[6]	Adjusted P-value[7]
3	b	TI	IgG1-Campath-RGE	IgG1-b12	ADCC	Wien-133	6	-2.90	5.40	84.95 to 120.8	<0.0001	-15.05 to 20.84	0.9910
3	b	TI	IgG1-11B8-AGK	IgG1-b12	ADCC	Wien-133	6	-3.44	5.31	85.50 to 121.4	<0.0001	-14.50 to 21.39	0.9805
3	b	TI	IgG1-Campath-RGE	IgG1-11B8-AGK	ADCC	Wien-133	6	1.72	5.21	80.33 to 116.2	<0.0001	-19.67 to 16.22	0.9987
3	b	NC	IgG1-b12	IgG1-b12	ADCC	Wien-133	6	0.00	5.37	82.06 to 117.9	<0.0001		
3	c	PC	IgG1-Campath-E430G	IgG1-11B8-E430G	ADCP	Raji	6	100.0	5.59			-106.5 to -93.54	<0.0001
3	c	TI	IgG1-Campath-RGE	IgG1-b12	ADCP	Raji	6	0.17	1.51	93.37 to 106.3	<0.0001	-6.628 to 6.291	>0.9999
3	c	TI	IgG1-11B8-AGK	IgG1-b12	ADCP	Raji	6	25.79	4.84	67.75 to 80.67	<0.0001	-32.25 to -19.33	<0.0001
3	c	TI	IgG1-Campath-RGE	IgG1-11B8-AGK	ADCP	Raji	6	39.16	5.83	54.38 to 67.30	<0.0001	-45.62 to -32.70	<0.0001
3	c	NC	IgG1-b12	IgG1-b12	ADCP	Raji	6	0.00	1.05	93.54 to 106.5	<0.0001		
3	d	PC	IgG1-Campath	IgG1-11B8	CDC	Wien-133	3	100.0	5.76			-113.7 to -86.29	<0.0001
3	d	TI	IgG1-Campath-E430G	IgG1-11B8-E430G	CDC	Wien-133	3	276.92	12.83	-192.4 to -161.5	<0.0001	-290.6 to -263.2	<0.0001
3	d	TI	IgG1-Campath-RGE	IgG1-b12	CDC	Wien-133	3	-12.51	2.78	97.04 to 128.0	<0.0001	-1.207 to 26.22	0.0808
3	d	TI	IgG1-11B8-AGK	IgG1-b12	CDC	Wien-133	3	3.86	7.82	80.68 to 111.6	<0.0001	-17.57 to 9.857	0.9091
3	d	TI	IgG1-Campath-RGE	IgG1-11B8-AGK	CDC	Wien-133	3	146.83	3.01	-62.29 to -31.36	<0.0001	-160.5 to -133.1	<0.0001
3	d	NC	IgG1-b12	IgG1-b12	CDC	Wien-133	6	0.00	5.17	86.61 to 113.4	<0.0001		
5	c	PC	Tit IgG1-Campath-RGE	Tit IgG1-11B8-AGK	CDC	Wien-133	3	100.0	2.91			ND	ND
5	c	TI	Tit IgG1-Campath-RGE	20 µg/mL IgG1-11B8-AGK	CDC	Wien-133	3	141.7	4.24	-50.01 to -33.39	<0.0001	ND	ND
5	c	TI	20 µg/mL IgG1-Campath-RGE	Tit IgG1-11B8-AGK	CDC	Wien-133	3	122.00	3.38	-30.31 to -13.70	0.0005	ND	ND
6	a	PC	IgG1-37.3-E430G	IgG1-11B8-E430G	CDC	Raji	3	100.0	3.69			-107.1 to -92.91	<0.0001
6	a	TI	IgG1-37.3-RGE	IgG1-b12	CDC	Raji	3	7.33	1.70	85.58 to 99.77	<0.0001	-14.42 to -0.2342	0.0428
6	a	TI	IgG1-11B8-AGK	IgG1-b12	CDC	Raji	3	4.26	1.60	88.65 to 102.8	<0.0001	-11.35 to 2.839	0.3028
6	a	TI	IgG1-37.3-RGE	IgG1-11B8-AGK	CDC	Raji	3	62.18	4.97	30.73 to 44.92	<0.0001	-69.27 to -55.08	<0.0001
6	a	NC	IgG1-b12	IgG1-b12	CDC	Raji	3	0.00	1.18	92.91 to 107.1	<0.0001		
6	c	PC	IgG1-DR5-01-E430G	IgG1-DR5-05-E430G	Apoptosis	COLO-205	3	100.0	2.38			-107.2 to -92.75	<0.0001
6	c	TI	IgG1-DR5-01-RGE	IgG1-b12	Apoptosis	COLO-205	3	10.57	2.94	82.18 to 96.67	<0.0001	-17.82 to -3.325	0.0059

Fig.	Sub	Item[1]	Antibody component 1	Antibody component 2	Assay	Cells	N[2]	Mean rel. AUC (%)[3]	SD	95% CI of diff. to PC[4]	Adjusted P-value[5]	95% CI of diff. to NC[6]	Adjusted P-value[7]
6	c	TI	IgG1-DR5-05-AGK	IgG1-b12	Apoptosis	COLO-205	3	6.19	2.50	86.56 to 101.1	<0.0001	-13.44 to 1.056	0.0990
6	c	TI	IgG1-DR5-01-RGE	IgG1-DR5-05-AGK	Apoptosis	COLO-205	3	86.02	4.87	6.733 to 21.23	0.0008	-93.27 to -78.77	<0.0001
6	c	NC	IgG1-b12	IgG1-b12	Apoptosis	COLO-205	3	0.00	1.70	92.75 to 107.2	<0.0001		
6	c	PC	IgG1-DR5-01-E430G	IgG1-DR5-05-E430G	Apoptosis	BxPC-3	3	100.0	8.60			-113.1 to -86.91	<0.0001
6	c	TI	IgG1-DR5-01-RGE	IgG1-b12	Apoptosis	BxPC-3	3	2.21	3.73	84.71 to 110.9	<0.0001	-15.29 to 10.88	0.9647
6	c	TI	IgG1-DR5-05-AGK	IgG1-b12	Apoptosis	BxPC-3	3	-10.72	2.66	97.63 to 123.8	<0.0001	-2.369 to 23.80	0.1164
6	c	TI	IgG1-DR5-01-RGE	IgG1-DR5-05-AGK	Apoptosis	BxPC-3	3	80.08	7.11	6.831 to 33.00	0.0045	-93.17 to -67.00	<0.0001
6	c	NC	IgG1-b12	IgG1-b12	Apoptosis	BxPC-3	3	0.00	2.88	86.91 to 113.1	<0.0001		
S2	a	PC	IgG1-Campath-E430G	IgG1-11B8-E430G	CDC	Wien-133	3	100.0	4.63			-105.5 to -94.52	<0.0001
S2	a	TI	IgG1-Campath-E430G	IgG1-b12	CDC	Wien-133	3	90.58	5.76	2.705 to 16.13	0.0039	-97.30 to -83.87	<0.0001
S2	a	TI	IgG1-11B8-E430G	IgG1-b12	CDC	Wien-133	3	15.03	2.90	78.26 to 91.68	<0.0001	-21.74 to -8.319	<0.0001
S2	a	TI	IgG1-Campath	IgG1-b12	CDC	Wien-133	3	25.79	0.81	67.50 to 80.92	<0.0001	-32.50 to -19.08	<0.0001
S2	a	TI	IgG1-11B8	IgG1-b12	CDC	Wien-133	3	-1.41	1.44	94.70 to 108.1	<0.0001	-5.299 to 8.124	0.9839
S2	a	TI	IgG1-Campath	IgG1-11B8	CDC	Wien-133	3	36.11	2.08	57.18 to 70.60	<0.0001	-42.82 to -29.40	<0.0001
S2	a	NC	IgG1-b12	IgG1-b12	CDC	Wien-133		0.00	1.87	94.52 to 105.5	<0.0001		
S2	b	PC	IgG1-Campath-E430G	x	CDC	Wien-133	3	100.0	2.77			-105.1 to -94.89	<0.0001
S2	b	TI	IgG1-Campath-E430G-K439E	x	CDC	Wien-133	3	40.63	1.59	55.19 to 63.54	<0.0001	-44.81 to -36.46	<0.0001
S2	b	TI	IgG1-Campath	x	CDC	Wien-133	3	43.84	2.01	51.05 to 61.27	<0.0001	-48.95 to -38.73	<0.0001
S2	b	TI	IgG1-Campath-K439E	x	CDC	Wien-133	3	0.76	1.03	94.13 to 104.3	<0.0001	-5.872 to 4.348	0.9722
S2	b	NC	IgG1-b12	x	CDC	Wien-133	3	0.00	1.45	94.89 to 105.1	<0.0001		
S3		PC	IgG1-Campath-E430G	x	CDC	Wien-133	3	100.0	1.22			ND	ND
S3		TI	IgG1-Campath	x	CDC	Wien-133	3	39.06	1.02	59.43 to 64.92	<0.0001	ND	ND
S3		TI	IgG1-Campath-G237A-E430G	x	CDC	Wien-133	3	74.06	1.08	-0.2705 to 5.211	0.0763	ND	ND
S3		TI	IgG1-Campath-G236R-E430G	x	CDC	Wien-133	3	98.76	0.47	24.43 to 29.92	<0.0001	ND	ND
S4		PC	IgG1-Campath-E430G	IgG1-11B8-E430G	FcγRIIa H131 activity	Raji	3	99.99	6.71			-107.2 to -92.81	<0.0001

Fig.	Sub	Item[1]	Antibody component 1	Antibody component 2	Assay	Cells	N[2]	Mean rel. AUC (%)[3]	SD	95% CI of diff. to PC[4]	Adjusted P-value[5]	95% CI of diff. to NC[6]	Adjusted P-value[7]
S4		TI	IgG1-Campath-RGE	IgG1-b12	FcγRIIa H131 activity	Raji	3	0.01	0.58	92.80 to 107.2	<0.0001	-7.188 to 7.173	>0.9999
S4		TI	IgG1-11B8-AGK	IgG1-b12	FcγRIIa H131 activity	Raji	3	-0.27	0.33	93.08 to 107.4	<0.0001	-6.917 to 7.445	0.9999
S4		TI	IgG1-Campath-RGE	IgG1-11B8-AGK	FcγRIIa H131 activity	Raji	3	1.20	0.82	91.61 to 106.0	<0.0001	-8.386 to 5.976	0.9652
S4		NC	IgG1-b12	IgG1-b12	FcγRIIa H131 activity	Raji	3	0.00	0.30	92.81 to 107.2	<0.0001		
S4		PC	IgG1-Campath-E430G	IgG1-11B8-E430G	FcγRIIIa V158 activity	Raji	3	99.99	2.33			-102.7 to -97.30	<0.0001
S4		TI	IgG1-Campath-RGE	IgG1-b12	FcγRIIIa V158 activity	Raji	3	1.03	0.98	96.27 to 101.7	<0.0001	-3.726 to 1.659	0.6487
S4		TI	IgG1-11B8-AGK	IgG1-b12	FcγRIIIa V158 activity	Raji	3	0.01	0.24	97.29 to 102.7	<0.0001	-2.701 to 2.683	>0.9999
S4		TI	IgG1-Campath-RGE	IgG1-11B8-AGK	FcγRIIIa V158 activity	Raji	3	0.17	0.16	97.13 to 102.5	<0.0001	-2.863 to 2.521	0.9990
S4		NC	IgG1-b12	IgG1-b12	FcγRIIIa V158 activity	Raji	3	0.00	0.17	97.30 to 102.7	<0.0001		
S5[8]		PC	IgG1-Campath	IgG1-11B8	C1q binding	Wien-133	6	100.0	41.07			-10.43 to -0.7746	0.0132
S5		TI	IgG1-Campath-E430G	IgG1-11B8-E430G	C1q binding	Wien-133	6	1859	87.50	-108.2 to -88.82	<0.0001	-114.4 to -93.85	<0.0001
S5		TI	IgG1-Campath-RGE	IgG1-b12	C1q binding	Wien-133	6	8.93	5.36	0.2520 to 9.948	0.0202	-1.092 to 0.09230	0.0629
S5		TI	IgG1-11B8-E430G-S440K	IgG1-b12	C1q binding	Wien-133	6	16.07	5.36	-0.1480 to 9.548	0.0284	-1.492 to -0.3077	0.0016
S5		TI	IgG1-11B8-AGK	IgG1-b12	C1q binding	Wien-133	6	5.36	3.57	0.4746 to 10.13	0.0168	-0.7511 to 0.1511	0.1945
S5		TI	IgG1-Campath-RGE	IgG1-11B8-E430G-S440K	C1q binding	Wien-133	6	287.5	39.29	-15.58 to -5.424	<0.0001	-20.72 to -11.48	<0.0001
S5		TI	IgG1-Campath-RGE	IgG1-11B8-AGK	C1q binding	Wien-133	6	92.86	19.64	-4.160 to 4.960	>0.9999	-7.537 to -2.863	0.0007
S5		NC	IgG1-b12	IgG1-b12	C1q binding	Wien-133	6	0.00	3.57	0.7746 to 10.43	0.0132		
S6		PC	IgG1-DR5-01-E430G	IgG1-DR5-05-E430G	Apoptosis	BxPC-3	3	100.0	1.10			-105.5 to -94.46	<0.0001

Fig.	Sub	Item[1]	Antibody component 1	Antibody component 2	Assay	Cells	N[2]	Mean rel. AUC (%)[3]	SD	95% CI of diff. to PC[4]	Adjusted P-value[5]	95% CI of diff. to NC[6]	Adjusted P-value[7]
S6		TI	IgG1-DR5-01	IgG1-DR5-05	Apoptosis	BxPC-3	3	55.13	3.64	39.33 to 50.41	<0.0001	-60.67 to -49.59	<0.0001
S6		NC	IgG1-b12	IgG1-b12	Apoptosis	BxPC-3	3	0.00	1.55	94.46 to 105.5	<0.0001		
S6		PC	IgG1-DR5-01-E430G	IgG1-DR5-05-E430G	Apoptosis	COLO-205	3	100.0	4.67			-111.6 to -88.39	<0.0001
S6		TI	IgG1-DR5-01	IgG1-DR5-05	Apoptosis	COLO-205	3	5.51	4.91	82.88 to 106.1	<0.0001	-17.12 to 6.105	0.3561
S6		NC	IgG1-b12	IgG1-b12	Apoptosis	COLO-205	3	0.00	5.31	88.39 to 111.6	<0.0001		

1 Items: positive control (PC), negative control (NC) or test item (TI) used in comparisons.

2 Number of independent experimental repeats, performed on separate days, using independently prepared antibody mixtures.

3 Dose-response data from multiple experimental repeats were pooled, concentrations were log-transformed and the resulting AUC values were normalized relative to the positive control indicated in grey (100%) and negative control non-binding antibody IgG1-b12 (0%).

4 95% confidence interval of the difference between measured value (test item) and value measured for positive control antibody or antibody mixture.

5 Adjusted p-value of one-way ANOVA analysis of difference between test item and positive control using Dunnett's multiple comparisons test. Analyses were performed using GraphPad Prism release 8.4.1.

6 95% confidence interval of the difference between test item and negative control values.

7 Adjusted P-value calculated as described *5, here for the difference between test item and negative control values. ND: not determined.

8 Dunnett's T3 multiple comparisons test was used to address the different standard deviations between groups.

Supplementary Table 4

Statistical analysis of Pharmacokinetics data

Fig.	Sub	Item[1]	Antibody component 1	Antibody component 2	Assay	Cells	N[2]	Clearance rate[3]	SD	95% CI of diff. to PC[3]	Adjusted P-value[4]
3	e	PC	IgG1-Campath	-	PK	N/A	3	28.8	6.7		
3	e	TI	IgG1-Campath-RGE	-	PK	N/A	3	34.6	7.3	-16.99 to 5.393	0.5862
3	e	PC	IgG1-11B8	-	PK	N/A	3	14	1.1		
3	e	TI	IgG1-11B8-AGK	-	PK	N/A	3	10.8	0.9	-14.39 to 7.993	0.9513
3	e	PC	IgG1-Campath	IgG1-11B8	PK	N/A	3	11.9	1.5		
3	e	TI	IgG1-Campath-RGE	IgG1-11B8-AGK	PK	N/A	3	11.8	1.9	-11.09 to 11.29	>0.9999

1 Items: positive control (PC) or test item (TI) used in comparisons.

2 Number of mice.

3 Clearance of a single antibody dose (500 µg) was monitored for three weeks and is expressed as Dose (D)*1000/area under the curve (ml/day/kg).

4 95% confidence interval of the difference between measured value (test item) and value measured for positive control antibody or antibody mixture.

5 Adjusted p-value of one-way ANOVA analysis of difference between test items and positive controls using Tukey's multiple comparisons test.